mouse. The standard feed used in this study and in the Laboratory Animal Facility of the National Institute of Neuroscience, NCNP, contains approximately two times the calcium, six times the potassium, six times the magnesium, seven times the sodium, and six times the zinc as the estimated minimal mineral requirements for mice (31). Hence, the mice in this study and at our institute may have ingested necessary calcium, sodium, and zinc in their diet to survive as long as B10 mice.

Our results suggest that blood Ca^{2+} concentration, muscle zinc content, and potassium excretion are important for the inhibition of muscle fiber necrosis in mdx mice.

In future studies, we will further investigate the cause-and-effect relationship of NaCl supplementation to identify effective therapies for reducing the rate of muscle degeneration and improving the quality of life of DMD patients.

ACKNOWLEDGMENTS

We give grateful thanks to Drs. O. Imazawa, A. Ishii, I. Kamo, and A. Takahashi [National Center of Neurology and Psychiatry (NCNP)], as well as M. Date (Riken) for helpful support and discussions; to S. Wakai (NCNP) for assistance measuring serum CK activity and to Prof. W. L. Stahl (University of Washington, Seattle) and Dr. I. Nonaka (NCNP) for critically reading the manuscript. Special thanks are also given to Prof. U. T. Ruegg (University of Geneva) for critical discussions, suggestions, and reading.

GRANTS

This work was supported in part by a grant-in-aid from the NCNP of the Ministry of Health, Labour and Welfare of Japan.

REFERENCES

1. **Balnave CD and Allen DG.** Evidence for Na+/Ca^{2+} exchange in intact single skeletal muscle fibers from the mouse. *Am J Physiol Cell Physiol* 274: C940–C946, 1998.
2. **Beam KG.** Duchenne muscular dystrophy. Localizing the gene product. *Nature* 333: 798–799, 1988.
3. **Bertorini TE, Bhattacharya SK, Palmieri GM, Chesney CM, Pifer D, and Baker B.** Muscle calcium and magnesium content in Duchenne muscular dystrophy. *Neurology* 32: 1088–1092, 1982.
4. **Bertorini TE, Cornelio F, Bhattacharya SK, Palmieri GM, Dones I, Dworzak F, Brambati B, Chesney CM, Pifer D, and Baker B.** Calcium and magnesium content in fetuses at risk and prenecrotic Duchenne muscular dystrophy. Muscle calcium and magnesium content in Duchenne muscular dystrophy. *Neurology* 34: 1436–1440, 1984.
5. **Bettger WJ and O'Dell BL.** Physiological roles of zinc in the plasma membrane of mammalian cells. *J Nutr Biochem* 4: 194–207, 1993.
6. **Bodensteiner JB and Engel AG.** Intracellular calcium accumulation in Duchenne dystrophy and other myopathies: a study of 567,000 muscle fibers in 114 biopsies. *Neurology* 28: 439–446, 1978.
7. **Bogin E, Massry SG, Levi J, Djaldeti M, Bristol G, and Smith J.** Effect of parathyroid hormone on osmotic fragility of human erythrocytes. *J Clin Invest* 69: 1017–1025, 1982.
8. **Buetler TM, Renard M, Offord EA, Schneider H, and Ruegg UT.** Green tea extract decreases muscle necrosis in mdx mice and protects against reactive oxygen species. *Am J Clin Nutr* 75: 749–753, 2002.
9. **Bukoski RD, Xue H, and McCarron DA.** Effect of 1,25(OH)2 vitamin D3 and ionized Ca2+ on 45Ca uptake by primary cultures of aortic myocytes of spontaneously hypertensive and Wistar-Kyoto normotensive rats. *Biochem Biophys Res Commun* 146: 1330–1335, 1987.
10. **Campbell KP and Kahl SD.** Association of dystrophin and an integral membrane glycoprotein. *Nature* 338: 259–262, 1989.
11. **Carpenter S and Karpati G.** Duchenne muscular dystrophy: plasma membrane loss initiates muscle cell necrosis unless it is repaired. *Brain* 102: 147–161, 1979.
12. **Collet C, Csernoch L, and Jacquemond V.** Intramembrane charge movement and L-type calcium current in skeletal muscle fibers isolated from control and mdx mice. *Biophys J* 84: 251–265, 2003.
13. **Deval E, Levitsky DO, Marchand E, Cantereau A, Raymond G, and Cognard C.** Na(+)/Ca(2+) exchange in human myotubes: intracellular calcium rises in response to external sodium depletion are enhanced in DMD. *Neuromuscul Disord* 12: 665–673, 2002.
14. **Dhalla NS, McNamara DB, Balasubramanian V, Greenlaw R, and Tucker FR.** Alterations of adenosine triphosphatase activities in dystrophic muscle sarcolemma. *Res Commun Chem Pathol Pharmacol* 6: 643–650, 1973.
15. **Emery AE.** Population frequencies of inherited neuromuscular diseases—a world survey. *Neuromuscul Disord* 1: 19–29, 1991.
16. **Engel AG, Yamamoto M, and Fischbeck KH.** Dystrophinopathies. In: *Myology* (2nd ed.), edited by Engel AG and Franzini-Armstrong, C. New York: McGraw-Hill, 1133–1187, 1994.
17. **Fisher I, Abraham D, Bouri K, Hoffman EP, Muntoni F, and Morgan J.** Prednisolone-induced changes in dystrophic skeletal muscle. *FASEB J* 19: 834–836, 2005.
18. **Fong PY, Turner PR, Denetclaw WF, and Steinhardt RA.** Increased activity of calcium leak channels in myotubes of Duchenne human and mdx mouse origin. *Science* 250: 673–676, 1990.
19. **Glesby MJ, Rosenmann E, Nylen EG, and Wrogemann K.** Serum CK, calcium, magnesium, and oxidative phosphorylation in mdx mouse muscular dystrophy. *Muscle Nerve* 11: 852–856, 1988.
20. **Gorospe JRM, Nishikawa BK, and Hoffman EP.** Pathophysiology of dystrophin deficiency: a clinical and biological enigma. In: *Dystrophin Gene, Protein and Cell Biology*, edited by Brown SC and Lucy JA: New York: Cambridge University Press, pp. 201–232, 1997.
21. **Goyenvalle A, Vulin A, Fougerousse F, Leturcq F, Kaplan JC, Garcia L, and Danos O.** Rescue of dystrophic muscle through U7 snRNA-mediated exon skipping. *Science* 306: 1796–1799, 2004.
22. **Harper SQ, Hauser MA, DelloRusso C, Duan D, Crawford RW, Phelps SF, Harper HA, Robinson AS, Engelhardt JF, Brooks SV, and Chamberlain JS.** Modular flexibility of dystrophin: implications for gene therapy of Duchenne muscular dystrophy. *Nat Med* 8: 253–261, 2002.
23. **Hubner C, Lehr HA, Bodlaj R, Finckh B, Oexle K, Marklund SL, Freudenberg K, Kontush A, Speer A, Terwolbeck K, Voit T, and Kohlschutter A.** Wheat kernel ingestion protects from progression of muscle weakness in mdx mice, an animal model of Duchenne muscular dystrophy. *Pediatr Res* 40: 444–449, 1996.
24. **Jackson MJ, Jones DA, and Edwards RH.** Measurements of calcium and other elements in muscle biopsy samples from patients with Duchenne muscular dystrophy. *Clin Chim Acta* 147: 215–221, 1985.
25. **Jin JY, Wen JF, Li D, and Cho KW.** Osmoregulation of atrial myocytic ANP release: osmotransduction via cross-talk between L-type Ca^{2+} channel and SR Ca^{2+} release. *Am J Physiol Regul Integr Comp Physiol* 287: R1101–R1109, 2004.
26. **Lijnen P and Petrov V.** Dietary calcium, blood pressure and cell membrane cation transport systems in males. *J Hypertens* 13: 875–882, 1995.
27. **Luttgau HC.** The action of calcium ions on potassium contractures of single muscle fibres. *J Physiol* 168: 679–697, 1963.
28. **Marchi Alves LM, Tosi LR, Antunes-Rodrigues J, and Carnio EC.** Is there a link between salt-intake and atrial natriuretic peptide system during hypertension induced by nitric oxide blockade? *Regul Pept* 120: 127–132, 2004.
29. **Maunder-Sewry CA, Gorodetsky R, Yarom R, and Dubowitz V.** Element analysis of skeletal muscle in Duchenne muscular dystrophy using x-ray fluorescence spectrometry. *Muscle Nerve* 3: 502–508, 1980.
30. **McArdle A, Edwards RH, and Jackson MJ.** Accumulation of calcium by normal and dystrophin-deficient mouse muscle during contractile activity in vitro. *Clin Sci (Lond)* 82: 455–459, 1992.
31. **National Research Council.** Nutrient requirements of the mouse. In: *Nutrient Requirements of Laboratory Animals*, Washington, D.C.: National Academy Press, chapt. 3, p. 80, 1995.
32. **Okinaka S, Kumagai H, Ebashi S, Sugita H, Momoi H, Toyokura Y, and Fujie Y.** Serum creatine phosphokinase. Activity in progressive muscular dystrophy and neuromuscular diseases. *Arch Neurol* 4: 520–525, 1961.
33. **Passaquin AC, Renard M, Kay L, Challet C, Mokhtarian A, Wallimann T, and Ruegg UT.** Creatine supplementation reduces skeletal muscle degeneration and enhances mitochondrial function in mdx mice. *Neuromuscul Disord* 12: 174–182, 2002.
34. **Reeve JL, McArdle A, and Jackson MJ.** Age-related changes in muscle calcium content in dystrophin-deficient mdx mice. *Muscle Nerve* 20: 357–360, 1997.

35. **Reineck HJ, Osgood RW, Ferris TF, and Stein JH.** Potassium transport in the distal tubule and collecting duct of the rat. *Am J Physiol* 229: 1403–1409, 1975.
36. **Shiramine K, Aou S, and Hori T.** Lateral hypothalamic injection of GABA(A) antagonist induces gastric vagus-mediated hypocalcemia in the rat. *Am J Physiol Regul Integr Comp Physiol* 273: R1492–R1500, 1997.
37. **Spencer MJ and Mellgren RL.** Overexpression of a calpastatin transgene in mdx muscle reduces dystrophic pathology. *Hum Mol Genet* 11: 2645–2655, 2002.
38. **Suh JG, Yamazaki A, and Tomita T.** Breeding of the gad-mdx mouse: influence of genetically induced denervation on dystrophic muscle fibers. *Lab Anim Sci* 44: 42–46, 1994.
39. **Sulakhe PV, Fedelesova M, McNamara DB, and Dhalla NS.** Isolation of skeletal muscle membrane fragments containing active Na+-K+ stimulated ATPase: comparison of normal and dystrophic muscle sarcolemma. *Biochem Biophys Res Commun* 42: 793–800, 1971.
40. **Takagi A, Watanabe T, Kojima S, and Endo Y.** Effect of long-term administration of prednisolone on serum creatine kinase and muscle pathology of mdx mouse. *Rinsho Shinkeigaku* 38: 724–728, 1998.
41. **Tameyasu T, Yamada M, Tanaka M, and Takahashi S.** Effect of zinc-carnosine chelate compound on muscle function in mdx mouse. *Jpn J Physiol* 52: 111–120, 2002.
42. **Tinsley JM, Potter AC, Phelps SR, Fisher R, Trickett JI, and Davies KE.** Amelioration of the dystrophic phenotype of mdx mice using a truncated utrophin transgene. *Nature* 384: 349–353, 1996.
43. **Wang Z, Zhu T, Qiao C, Zhou L, Wang B, Zhang J, Chen C, Li J, and Xiao X.** Adeno-associated virus serotype 8 efficiently delivers genes to muscle and heart. *Nat Biotechnol* 23: 321–328, 2005.
44. **Watkins SC, Hoffman EP, Slayter HS, and Kunkel LM.** Immunoelectron microscopic localization of dystrophin in myofibres. *Nature* 333: 863–866, 1988.
45. **Winegar BD and Lansman JB.** Voltage-dependent block by zinc of single calcium channels in mouse myotubes. *J Physiol* 425: 563–578, 1990.
46. **Yilmaz O, Karaduman A, and Topaloglu H.** Prednisolone therapy in Duchenne muscular dystrophy prolongs ambulation and prevents scoliosis. *Eur J Neurol* 11: 541–544, 2004.
47. **Yoshida M, Matsuzaki T, Date M, and Wada K.** Skeletal muscle fiber degeneration in mdx mice induced by electrical stimulation. *Muscle Nerve* 20: 1422–1432, 1997.
48. **Zatz M, Shapiro LJ, Campion DS, Oda E, and Kaback MM.** Serum pyruvate-kinase (PK) and creatine-phosphokinase (CPK) in progressive muscular dystrophies. *J Neurol Sci* 36: 349–362, 1978.
49. **Zemel MB, Bedford BA, Zemel PC, Marwah O, and Sowers JR.** Altered cation transport in non-insulin-dependent diabetic hypertension: effects of dietary calcium. *J Hypertens Suppl* 6: S228–S230, 1988.

MOLECULAR AND CELLULAR BIOLOGY, Nov. 2005, p. 9973–9984 Vol. 25, No. 22
0270-7306/05/$08.00+0 doi:10.1128/MCB.25.22.9973–9984.2005

Phosphorylation by Rho Kinase Regulates CRMP-2 Activity in Growth Cones

Nariko Arimura,[1,2] Céline Ménager,[1] Yoji Kawano,[1,5] Takeshi Yoshimura,[1] Saeko Kawabata,[1] Atsushi Hattori,[1] Yuko Fukata,[1] Mutsuki Amano,[1] Yoshio Goshima,[3] Masaki Inagaki,[2] Nobuhiro Morone,[4] Jiro Usukura,[4] and Kozo Kaibuchi[1]*

Department of Cell Pharmacology, Graduate School of Medicine, Nagoya University, 65 Tsurumai, Showa, Nagoya, Aichi 466-8550, Japan[1]; Division of Biochemistry, Aichi Cancer Center Research Institute, 1-1 Kanokoden, Chikusa, Nagoya, Aichi 464-8681, Japan[2]; Department of Molecular Pharmacology and Neurobiology, Yokohama City University School of Medicine, 3-9 Fukuura, Kanazawa, Yokohama 236-0004, Japan[3]; Department of Anatomy, School of Medicine, Nagoya University, 65 Tsurumai, Showa, Nagoya, Aichi 466-8550, Japan[4]; and Division of Molecular and Cell Biology, Institute for Medical Science, Dokkyo University School of Medicine, 880 Kitakobayashi, Mibumachi, Tochigi 321-0293, Japan[5]

Received 18 May 2005/Returned for modification 27 June 2005/Accepted 29 August 2005

Collapsin response mediator protein 2 (CRMP-2) enhances the advance of growth cones by regulating microtubule assembly and Numb-mediated endocytosis. We previously showed that Rho kinase phosphorylates CRMP-2 during growth cone collapse; however, the roles of phosphorylated CRMP-2 in growth cone collapse remain to be clarified. Here, we report that CRMP-2 phosphorylation by Rho kinase cancels the binding activity to the tubulin dimer, microtubules, or Numb. CRMP-2 binds to actin, but its binding is not affected by phosphorylation. Electron microscopy revealed that CRMP-2 localizes on microtubules, clathrin-coated pits, and actin filaments in dorsal root ganglion neuron growth cones, while phosphorylated CRMP-2 localizes only on actin filaments. The phosphomimic mutant of CRMP-2 has a weakened ability to enhance neurite elongation. Furthermore, ephrin-A5 induces phosphorylation of CRMP-2 via Rho kinase during growth cone collapse. Taken together, these results suggest that Rho kinase phosphorylates CRMP-2, and inactivates the ability of CRMP-2 to promote microtubule assembly and Numb-mediated endocytosis, during growth cone collapse.

Axon guidance is essential for the complexity of brain circuitry. Growth cones are thought to be a sensor for guidance molecules during development. Growth cones localize at the tips of axons and dynamically change their morphology in response to attractive and repulsive guidance cues, thus determining the direction of growth (16). Such morphological changes in growth cones are thought to be achieved by cytoskeleton reorganization, cell adhesion, and endocytosis (55, 64). Growth cones consist of actin filaments at the edge and microtubules and neurofilaments at the center. Recently, it was revealed that actin filaments are regulated during growth cone collapse induced by repulsive guidance cues (23). Furthermore, microtubules and endocytosis regulate growth cone morphology (11, 18, 26, 30, 43, 51). However, signal cascades regulating microtubules and endocytosis remain to be clarified.

Recent evidence supports the idea that cytoskeletal components are required for proper axonal path finding, and these components are regulated by members of the Rho family, including RhoA, Rac1, and Cdc42 (32, 36). Rho proteins serve as molecular switches by cycling between an inactive GDP-bound state and an active GTP-bound state (35, 42). In their active state, these GTPases bind characteristic sets of effector proteins. The most important effector of RhoA in the growth cone is probably the serine-threonine kinase, Rho-associated kinase (Rho kinase)/ROKα/ROCKII (5, 9, 74). Rho kinase binds to and is activated by the GTP-bound active form of Rho (2, 40).

Several research groups, including ours, support the idea that Rho kinase is a negative regulator of neurite formation and growth cone motility in neuronal cells downstream of Rho (1, 5, 38, 71). The ephrins, ligands of Eph receptor tyrosine kinases, have also been reported as a repulsive guidance cue to activate the Rho/Rho kinase signaling cascade during growth cone collapse (13, 71). The roles of the Eph family and ephrins in axon guidance have been studied in topographically organized sensory systems such as the retinotectal projection (21, 24, 46, 72). Activation of Eph receptor by, for example, ephrin-A5 causes the turning or collapse of growth cones. Analysis of the underlying signaling cascade has led to the identification of signaling molecules, such as ephexin, a Rho-specific guanine nucleotide exchange factor, which directly binds to Eph receptor and mediates signal from receptor to RhoA (44, 61, 63). In addition, myosin light chain (MLC) has been identified as one of the major substrates of Rho kinase-mediated growth cone collapse (1, 71). However, it is still unknown whether MLC phosphorylation is sufficient to mimic growth cone collapse induced by extracellular signals such as ephrin-A5 (71).

We previously identified collapsin response mediator protein 2 (CRMP-2) as a substrate of Rho kinase in the brain (5).

* Corresponding author. Mailing address: Department of Cell Pharmacology, Graduate School of Medicine, Nagoya University, 65 Tsurumai, Showa, Nagoya, Aichi 466-8550, Japan. Phone: 81 52 744 2074. Fax: 81 52 744 2083. E-mail: kaibuchi@med.nagoya-u.ac.jp.

CRMP-62, the chick CRMP-2 (98% identity), is reported to be required for the growth cone collapse of dorsal root ganglion (DRG) neurons induced by a repulsive guidance cue, semaphorin-3A (Sema3A; also known as collapsin-1) (30). UNC-33, the *Caenorhabditis elegans* homologue (30% homology), is identified by a mutation resulting in severely uncoordinated movement, abnormalities in axon guidance, and a superabundance of microtubules in neurons (37, 49). These results indicate that CRMP-2 is also a major mediator of growth cone collapse induced by repulsive guidance cues. We and other groups have reported that CRMP-2 is phosphorylated by Cdk5 and GSK-3β downstream of Sema3A (10, 14, 68, 73). This phosphorylation of CRMP-2 is essential for Sema3A-induced growth cone collapse (10). However, the exact roles of CRMP-2 phosphorylation remain to be clarified.

We recently identified two molecules, tubulin heterodimer and Numb, as CRMP-2-interacting molecules (28, 34). CRMP-2 shows much higher affinity to tubulin heterodimers than the polymerized tubulin (microtubules). CRMP-2 copolymerizes with tubulin dimers into microtubules and promotes tubulin polymerization in vitro. Furthermore, the overexpression of CRMP-2 facilitates the rate of axonal growth, whereas the mutant lacking the activity of the microtubule assembly inhibits axonal growth. Given the enriched localization of CRMP-2 in growing axons, it is likely that the CRMP-2–tubulin complex concentrated in the distal part of the axon promotes microtubule assembly and axon formation (28). CRMP-2 participates in Numb-mediated endocytosis and regulates L1 recycling at the growth cone, followed by axon elongation (56). Thus, CRMP-2 basically has positive effects on axon growth. These results raise the possibility that modification, such as phosphorylation, of CRMP-2 regulates the CRMP-2 activity in axon growth or growth cone dynamics, including growth cone collapse.

Here, we report that phosphorylation by Rho kinase diminishes the CRMP-2 activity with respect to binding to tubulin dimer and Numb in neurons. Such phosphorylation by Rho kinase is observed during ephrin-A5-induced growth cone collapse. These results suggest that phosphorylation of CRMP-2 by Rho kinase enhances growth cone collapse by inhibiting the ability of CRMP-2 to associate with microtubules and Numb.

MATERIALS AND METHODS

Materials and chemicals. cDNA encoding human CRMP-2 was obtained as described previously (5). CRMP-2 was subcloned into pB-GEX (rearranged vector from pGEX) or pRSET-C1 (Invitrogen Corp., Carlsbad, CA) to obtain the construct of CRMP-2 with glutathione *S*-transferase (GST) tagged at the C terminus of the protein or with His tagged at the N terminus of the protein. pEF-ephrin-A5/RAGS-Fc was kindly provided by Hideaki Tanaka (Kumamoto University) (57). The following antibodies were used: anti-CRMP-2 monoclonal antibody (C4G), kindly provided by Yasuo Ihara (Tokyo University) (33); anti-CRMP-2 polyclonal antibody raised against GST-CRMP-2; anti-phospho-CRMP-2 antibody (pT555 and pT514) raised against chemically synthesized phosphopeptides which are exactly identical to the amino acid sequence of chick CRMP-2, namely, CRMP-62 (5, 31, 73); anti-GST polyclonal antibody raised against GST; anti-Numb polyclonal antibody raised against 20-amino-acid residues at the C terminus of Numb; anti-myc polyclonal antibody (Santa Cruz Biotechnology Inc., CA); anti-Rho-GDI polyclonal antibody (Santa Cruz); anti-actin monoclonal antibody (clone C4; Chemicon International, Temecula, Calif.); anti-α-tubulin monoclonal antibody (DM1A; Sigma, St. Louis, MO); and anti-unique β-tubulin monoclonal antibody (TUJ1; Berkeley Antibody Company, Berkeley, CA). N1E-115 cells were kindly provided by Taiji Kato (Nagoya City University Medical School, Nagoya, Japan). Vero cells were kindly provided by Eisuke Mekada (Osaka University, Osaka, Japan). Y-27632 was provided by Mitsubishi Pharma Co. (Osaka, Japan). Other materials and chemicals were obtained from commercial sources.

Protein purification. Tubulin heterodimer was prepared from bovine brain by three cycles of polymerization and depolymerization followed by DEAE-Sepharose column chromatography using fast protein liquid chromatography (Amersham Biosciences Corp., Piscataway, NJ). Native bovine CRMP-2 was purified from bovine brain extracts by a method described previously (5). His-tagged CRMP-2 and GST-tagged CRMP-2 (CRMP-2-GST) were purified following the procedures recommended by Invitrogen Corp.

Phosphorylation assay. The phosphorylation assay of the samples was carried out as described previously (52). In brief, the kinase reaction for Rho kinase was performed in 50 μl of a reaction mixture (102 mM PIPES at pH 6.8, 1 mM EDTA, 1 mM dithiothreitol, 1.55 mM $MgSO_4$, 100 μM [γ-^{32}P]ATP [1 to 20 GBq/μmol], 100 nM purified GST-Rho kinase catalytic domain [RhoK-cat]) for 30 min at 30°C. RhoK-cat was produced in Sf9 cells with a baculovirus system and purified on glutathione-Sepharose 4B beads (Amersham Biosciences Corp.). GSK-3β and Cdk5 were obtained from Upstate Biotech (Charlottesville, VA). Then, the reaction mixtures were boiled in sodium dodecyl sulfate (SDS) sample buffer and subjected to SDS-polyacrylamide gel electrophoresis (SDS-PAGE) for estimation of the stoichiometry. The radiolabeled bands were visualized by an image analyzer (BAS 2000; Fujifilm, Tokyo, Japan).

In vitro binding assay. We first immobilized 0.5 μM phosphorylated or nonphosphorylated CRMP-2 onto glutathione-Sepharose 4B beads for 60 min at 4°C. To examine the interaction of CRMP-2 and tubulin heterodimers, the immobilized CRMP-2 with beads was incubated with 1.0 μM tubulin heterodimer for 120 min at 4°C. After removal of the supernatant of the CRMP-2–tubulin mixture, the beads were washed three times with PEM buffer (100 mM PIPES at pH 6.8, 1 mM EGTA, 0.5 mM $MgSO_4$). Then the samples were boiled in SDS sample buffer and subjected to SDS-PAGE and immunoblot analysis with the indicated antibodies. To examine the interaction of CRMP-2 with other molecules, the immobilized CRMP-2 was incubated with rat brain (P6 and P7) lysate in lysis buffer (20 mM Tris-HCl at pH 8.0, 150 mM NaCl, 1 mM EDTA, 1 mM phenylmethylsulfonyl fluoride, 10 μg/ml leupeptin, 10 μg/ml aprotinin, 1.0% NP-40, 1 μM calyculin A) for 60 min at 4°C. After removal of the supernatant, the beads were washed three times with washing buffer (20 mM Tris-HCl at pH 8.0, 150 mM NaCl, 1 mM EDTA, 1.0% NP-40). Then the samples were boiled in SDS sample buffer and subjected to SDS-PAGE and immunoblot analysis with the indicated antibodies.

Surface plasmon resonance measurements. Anti-α-tubulin monoclonal antibody (DM1A) was covalently coupled to a CM5 sensor chip in a Biacore 3000 system (Biacore, Tokyo, Japan) according to the manufacturer's instructions. Purified tubulin heterodimer (0.5 μM) was captured at a flow rate of 10 μl/min for 3 min. The level of resonance units raised by the addition of anti-tubulin antibodies was about 1,800 to 2,000 in each condition. Binding of 8, 4, 2, 1, and 0.5 μM phosphorylated or nonphosphorylated His-CRMP-2 to a sensor chip surface loaded with tubulin heterodimer was done in 100 mM PIPES (pH 6.8)–150 mM NaCl–3 mM EDTA–0.005% (wt/vol) Tween 20. Injection of each sample was programmed separately. Association was monitored over 3 min at a flow rate of 20 μl/min. The data were analyzed with the BIAevaluation 3.0 software (Biacore).

Cosedimentation assay. Tubulin (10 μM) was first assembled with 1 mM GTP, 10% dimethyl sulfoxide, and 20 μM Taxol for 30 min at 37°C. The assembled microtubules were mixed with 5 μM bovine serum albumin (BSA) or 5 μM phosphorylated or nonphosphorylated His-tagged CRMP-2 in PEM buffer. This mixture was incubated at 37°C for 10 min and centrifuged at 100,000 × *g* for 10 min at 37°C. The pellet and supernatant were subjected to SDS-PAGE.

Cell culture and transfection. Vero cells and N1E-115 cells were seeded on 13-mm round glass coverslips at 1.5×10^4 cells/mm^2 for immunostaining and cultured in Dulbecco's modified Eagle's medium containing 10% fetal bovine serum in an atmosphere of 5% CO_2 at 37°C. For transfection, Vero and N1E-115 cells were seeded and cultured overnight. Transfection of plasmids was carried out using Lipofectamine 2000 (Invitrogen) for Vero cells or Lipofectamine (Invitrogen) for N1E-115 cells. Chick DRG neurons were dissociated from 7-day-old chick embryos by use of papain as described previously (8). They were then seeded on 13-mm round glass coverslips coated with laminin at 1.5×10^4 cells/mm^2 in 24-well plates for immunostaining or on 35-mm culture dishes coated with laminin at 1.5×10^4 cells/mm^2 for immunoblot analysis. The cells were cultured in Dulbecco's modified Eagle's medium containing 100 ng/ml 2.5S nerve growth factor (NGF; Upstate Biotech) and 10% fetal bovine serum in an atmosphere of 5% CO_2. DRG neurons were prepared and transfected with the indicated plasmids by use of the calcium phosphate method before plating, as described previously (5). The transfection efficiency is about 1 to 2% using the

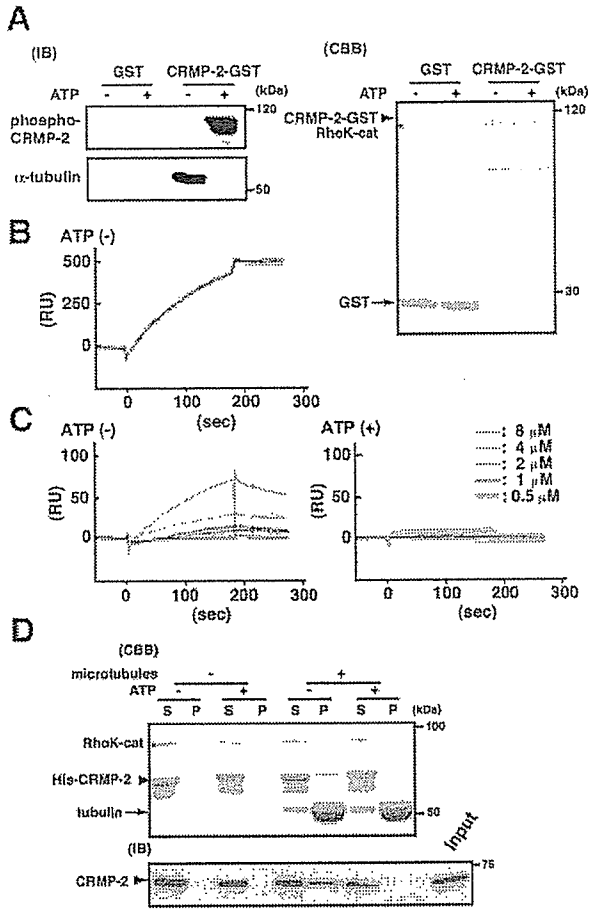

FIG. 1. An in vitro tubulin or microtubule binding assay using phosphorylated or nonphosphorylated CRMP-2-GST. (A) GST and CRMP-2-GST (0.5 μM) were phosphorylated by Rho kinase catalytic domain (RhoK-cat) in the presence (+) or absence (−) of ATP. GST or CRMP-2-GST immobilized onto beads was incubated with 1 μM tubulin in PEM buffer for 1 h at 4°C. GST and CRMP-2-GST results were shown with a Coomassie brilliant blue (CBB)-stained gel (right panel). Purified CRMP-2-GST contained degradation products, as confirmed by immunoblotting (IB) with anti-GST and anti-CRMP-2 antibody. An asterisk indicates RhoK-cat. An arrowhead and an arrow indicate the intact protein of CRMP-2-GST and GST, respectively. Phosphorylated CRMP-2-GST or the bound tubulin was analyzed by immunoblotting with anti-phospho-CRMP-2 antibody and anti-α-tubulin antibody (left panels). (B) Biacore sensorgram of tubulin capture with anti-tubulin antibody. Purified tubulin heterodimer (0.5 μM) was captured with the anti-α-tubulin antibody immobilized over the sensor chip at a flow rate of 10 μl/min for 3 min. The sensorgram in the sample of nonphosphorylated CRMP-2 [ATP (−)] is identical to that obtained with phosphorylated CRMP-2 [ATP (+)] (data not shown). The increase in RU (resonance units) results from the binding of tubulins to anti-tubulin antibodies. (C) Biacore sensorgram of CRMP-2 binding to tubulin. Binding of 8, 4, 2, 1, and 0.5 μM phosphorylated [ATP (+)] or nonphosphorylated [ATP (−)] His-CRMP-2 to a tubulin heterodimer-loaded sensor chip surface was examined. (D) Cosedimentation analysis of phospho-CRMP-2 or non-phospho-CRMP-2. His-CRMP-2 (5 μM) was phosphorylated by Rho kinase (RhoK-cat) in the presence (+) or absence (−) of ATP. His-CRMP-2 was mixed with 10 μM microtubules stabilized by Taxol (+) or left unmixed (−). After a 10-min incubation at 37°C, mixtures containing microtubules were centrifuged at 37°C. The quantity of His-CRMP-2 in supernatant (S) or pellet (P) was shown by Coomassie brilliant blue gel staining results (upper panel). The samples were analyzed by immunoblotting using anti-GST antibody to confirm the identity of this band as CRMP-2 (lower panel). An asterisk indicates RhoK-cat. An arrowhead and an arrow indicate His-CRMP-2 and tubulin, respectively.

calcium phosphate method with chick DRG neurons. The mean level of ectopic CRMP-2 expression is maximally fivefold that of the endogenous levels 3 days after transfection. For the analysis of axon length, we cultured DRG neurons without NGF. Spontaneous axon elongation was observed, probably because of the trophic factors secreted from contaminated neurotrophic cells or neurons.

Immunofluorescence study and microscopic observation. Vero cells, N1E-115 cells, and DRG neurons were fixed with 3.7% formaldehyde in phosphate-buffered saline (PBS) for 10 min at room temperature and then treated with 0.05% Triton X-100 for 10 min at 4°C. They were then treated with 1% BSA in PBS for 1 h at room temperature and incubated with the indicated antibodies. Immunoreactivity was visualized by incubation with fluorescein isothiocyanate (FITC)-conjugated anti-rabbit or mouse immunoglobulin antibodies (Amersham Biosciences Corp.) and Texas Red-conjugated anti-rabbit or mouse immunoglobulin antibodies (Amersham Biosciences Corp.). The images of immunostained cells or neurons were analyzed using a confocal laser microscopy system (LSM 510; Carl Zeiss, Oberkochen, Germany). Intensity of fluorescence was analyzed using the LSM 510 software.

For electron microscopic immunocytochemistry, DRG growth cones cultured on coverslips were fixed with 2% glutaraldehyde in 0.85 M cacodylate buffer adjusted to pH 7.4. Fixed samples were then dehydrated with an ascending series of ethanol up to 99.5% and embedded in Lowicryl K4M resin (Polysciences, Inc., Warrington, PA) according to the manufacturer's protocol. Immunolabeling was performed on the sections as described previously (50, 70).

For freeze-etching immunoreplica methods, growth cones cultured on large coverslips (13 × 13 mm) were washed once with PIPES buffer containing 10 mM PIPES, 100 mM KCl, 8 mM $MgCl_2$, and 3 mM EGTA. Small coverslips (5 × 5 mm) treated with alcian blue were placed on the growth cone-rich areas in a culture dish under the microscope. A fixative consisting of 1% glutaraldehyde and 2% paraformaldehyde in PIPES buffer was added immediately. Then coverslips were lifted slowly. In this way, apical plasma membranes of growth cones and axons were separated from the cytoplasm. After being washed with the buffer, isolated membranes attached to the coverslip were incubated with primary antibody raised against CRMP-2 or phosphorylated CRMP-2 in the PIPES buffer containing 1% BSA for 1 h. Samples were then labeled with 10 nm gold-conjugated secondary antibody (Amersham Biosciences Corp.) after being washed three times with the buffer for 1 h. After immunolabeling, specimens were rapidly frozen by plunging them onto a copper block cooled with liquid helium. Frozen specimens were brought into a freeze replica device (FR9000; Hitachi Science, Tokyo, Japan), slightly dried, and rotary shadowed with platinum and carbon. Shadowed specimens were removed from the coverslip in 5% hydrofluoric acid solution and observed under an electron microscope (1200 EX; JEOL Ltd., Tokyo, Japan).

Collapse assay. Both the transfected neurons and nontransfected neurons were cultured in serum plus medium for 20 h and then cultured in serum-free medium without NGF for 4 h. The collapse assay was performed as previously described (59). For the immunoblot analysis and the count of collapsed growth cones, neurons were stimulated with 1 μg/ml purified ephrin-A5-Fc. Although we know that the DRG neuron is not a common choice for studies of ephrin-A5, we used the same experimental system in a previous study employing Sema3A and lysophosphatidic acid (LPA) to obtain comparable results for ephrin-A5. It is reported that EphA2 and ephexin, a Rho nucleotide exchange factor, are expressed in DRG neurons (29, 61) and that DRG neurons react to ephrin-A5 and ephrin-A3 (19, 48). We observed better responses of ephrin-A5-stimulated DRG neurons in the absence of serum compared to those seen in the presence of serum. The pretreatment with 10 μM Rho kinase inhibitor (Y-27632 or HA1077) was performed for 1 h before the collapse assay. For immunoblot analysis, the cells were stimulated by ephrin-A5 for 3, 10, or 30 min at 37°C in serum-free medium without NGF. The cells were treated with 10% (wt/vol) trichloroacetic acid. The resulting precipitates were subjected to immunoblot analysis using anti-phospho-CRMP-2 and anti-CRMP-2 monoclonal antibody.

RESULTS

We previously showed that CRMP-2 binds to the tubulin dimer and enhances microtubule formation (28). We examined whether phosphorylation of CRMP-2 affects its tubulin binding

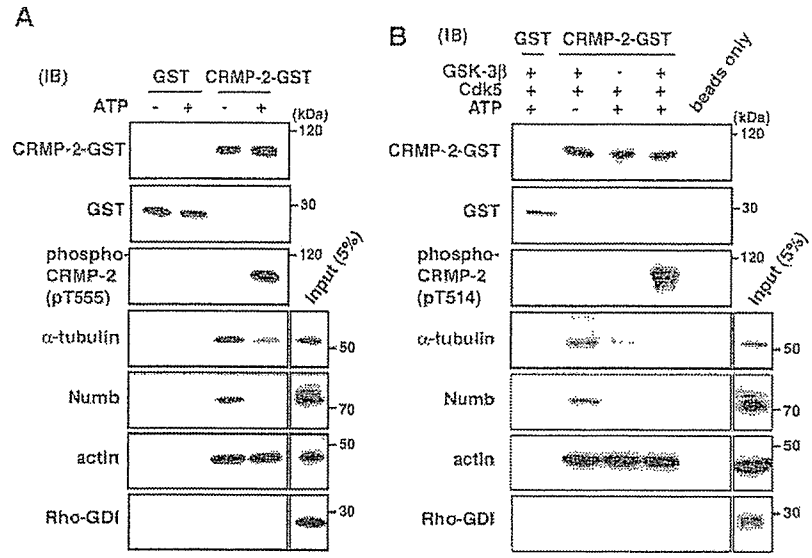

FIG. 2. An in vitro binding assay using phospho- or non-phospho-CRMP-2-GST and rat brain lysate. (A and B) GST and CRMP-2-GST (0.5 μM) were phosphorylated by Rho kinase catalytic domain (RhoK-cat) (A) or Cdk5 and/or GSK-3β (B) in the presence (+) or absence (−) of ATP. GST and CRMP-2-GST immobilized on beads were incubated with extracts of rat brain (P6 and P7) for 1 h at 4°C. CRMP-2-GST and the bound proteins were analyzed by immunoblotting (IB) using anti-GST antibody, anti-phospho-CRMP-2 antibody, anti-α-tubulin antibody, anti-Numb antibody, anti-Rho-GDI antibody, or anti-actin antibody. Input, immunoreactive bands of brain lysate (5% in total lysate). The lane labeled "beads only" shows the results for beads and brain lysates without GST proteins.

activity in vitro. Purified CRMP-2-GST was phosphorylated by RhoK-cat in the presence or absence of ATP. Phosphorylated CRMP-2 was detected by anti-phospho-CRMP-2 antibody, which specifically recognizes the phosphorylated state of CRMP-2 at Thr-555 (5) (Fig. 1A). Phosphorylated or nonphosphorylated CRMP-2 was immobilized on GST beads and incubated with purified tubulin heterodimer at 4°C. Tubulin was retained on the beads coated with nonphosphorylated CRMP-2, as reported previously (28), but not on the beads coated with phosphorylated CRMP-2 (Fig. 1A). The perturbation of the association of tubulin and CRMP-2 by phosphorylation was also confirmed by using the Biacore system (Fig. 1B and C). CRMP-2 bound to the retained tubulin in the Biacore sensor chip in a dose-dependent manner, whereas phosphorylated CRMP-2 did not (Fig. 1C). These results indicate that CRMP-2 phosphorylated by Rho kinase does not bind to the tubulin heterodimer.

We next examined whether phosphorylation of CRMP-2 affects its binding activity to microtubules in vitro (Fig. 1D) by use of a standard cosedimentation assay. Phosphorylated CRMP-2 or nonphosphorylated CRMP-2 was incubated with microtubules polymerized by Taxol at 37°C, and these mixtures were centrifuged to sediment the filamentous microtubules and the interacting molecules. BSA, a control protein, did not cosediment with microtubules (data not shown). Some nonphosphorylated CRMP-2 cosedimented with Taxol-stabilized microtubules, as reported previously (28). However, phosphorylated CRMP-2 was only minimally cosedimented. These results indicate that phosphorylation of CRMP-2 by Rho kinase decreases the ability of CRMP-2 to associate with microtubules as well as with tubulin heterodimers.

We next examined the effect of phosphorylation on the interaction of CRMP-2 with other molecules. We previously found that Numb binds to CRMP-2 directly and is localized at the axonal growth cone in neurons (56). The Numb and CRMP-2 complex mediates the endocytosis of L1 in the axonal growth cones, and Numb-mediated endocytosis of L1 is necessary for axon growth (56). We examined the interaction of phosphorylated CRMP-2 with partner proteins, including Numb, by a GST pulldown assay using rat brain lysate (Fig. 2A and B). Phosphorylated or nonphosphorylated CRMP-2 was immobilized on GST beads and incubated with postnatal rat brain lysate. An association of Numb with the beads coated with CRMP-2-GST was observed but not with the beads of phosphorylated CRMP-2-GST at Thr-555, suggesting that CRMP-2 phosphorylated by Rho kinase loses the ability to bind to Numb as well as tubulin (Fig. 2A). A small amount of tubulin was retained by phosphorylated CRMP-2 under these conditions, presumably because the high concentration of tubulin (approximately 13 μM) in brain lysates increased the efficiency of tubulin binding to phosphorylated CRMP-2 (Fig. 2A). Rho-GDI (a cytosolic and abundant protein used as a negative control) did not associate with CRMP-2. In addition, we identified actin as a CRMP-2-interacting molecule (Fig. 2A). Actin bound to phosphorylated CRMP-2 as well as to nonphosphorylated CRMP-2. These results indicate that CRMP-2 phosphorylation at the C terminus affects the interaction with certain proteins, including Numb and tubulin, but not with actin.

CRMP-2 can be phosphorylated by Cdk5 at Ser-522, and by recognizing this priming phosphorylation, GSK-3β phosphorylates CRMP-2 at Ser-518 and Thr-514 (10, 14, 68, 73). Since these phosphorylation sites are close to the phosphorylation site of Rho kinase, we examined whether these phosphorylations affect the association of CRMP-2 and interacting molecules. Similarly to Rho kinase results, the phosphorylation by

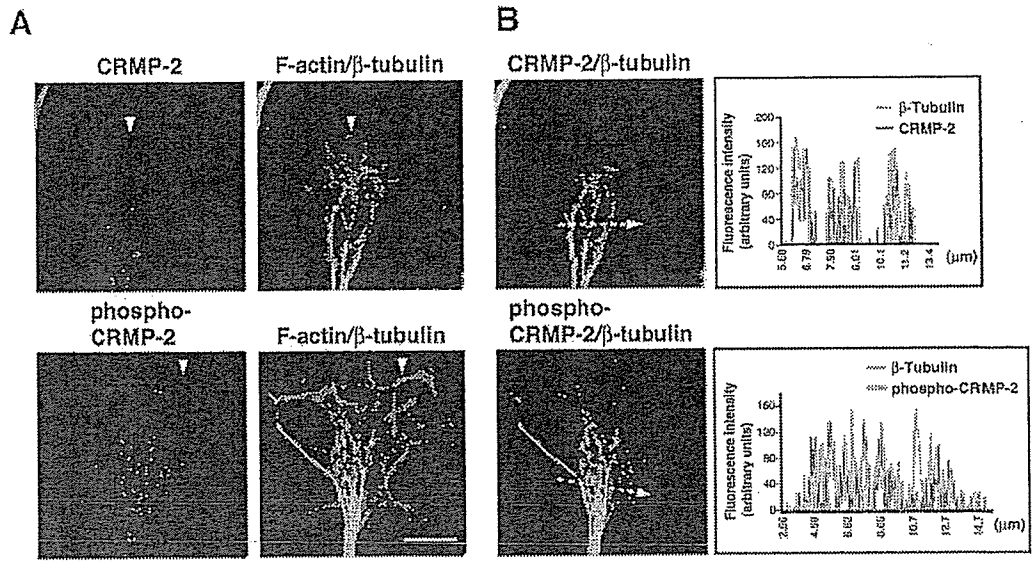

FIG. 3. Localization of CRMP-2 or phospho-CRMP-2 in chick DRG neuron growth cones. (A) Chick DRG neuron growth cones were triple stained with anti-CRMP-2 antibody (red), anti-unique β-tubulin antibody (green), and Alexa-649-phalloidin (blue) (upper panels) or anti-phospho-CRMP-2 antibody (red), anti-unique β-tubulin antibody (green), and Alexa-488-phalloidin (blue) (lower panels). Arrowheads indicate the colocalization of phosphorylated CRMP-2 or CRMP-2 and actin filaments. (B) Graphs plot the fluorescence intensity of immunolabeled CRMP-2 (red) and unique β-tubulin (green) or phosphorylated CRMP-2 (red) and unique β-tubulin (green) in the dotted line shown in each growth cone image. Bar, 10 μm.

Cdk5 and GSK-3β also prevents the binding of tubulin dimers and Numb but not that of actin (Fig. 2B). These results indicate that CRMP-2 phosphorylation at the C terminus by Rho kinase, Cdk5, and GSK-3β has similar effects on CRMP-2 function.

Next we examined the localization of CRMP-2 at DRG neuron growth cones. As reported previously, CRMP-2 is accumulated at the distal part of axons and growth cones (39, 54, 58). To examine the intracellular localization of phosphorylated CRMP-2 and interacting molecules, we performed an indirect immunofluorescence study using anti-phospho-CRMP-2 antibody (Fig. 3A). CRMP-2 immunoreactivity was mainly localized at the center of the growth cones and partially colocalized with microtubules and actin, as reported previously (56, 75). However, phosphorylated CRMP-2 was localized on punctate structures all around the growth cone area and some was seen even in the filopodia of the growth cones, which was stacked with actin filaments. Because phosphorylated CRMP-2 was present in all areas of growth cone, its immunoreactivity was overlapped with the filamentous image of microtubules. Localization of phosphorylated CRMP-2 itself did not appear to occur in the form of microtubule-like bundles or filaments, however, as was observed in experiments with anti-CRMP-2 antibody (Fig. 3B).

Subcellular localization of CRMP-2 in chick DRG growth cones was also examined by electron microscopic immunocytochemistry. As shown in immunofluorescence images (Fig. 3), microtubules were stuck and distributed in parallel. Immunolabeling in the electron micrograph was found predominantly on the filamentous image of microtubules but rarely in the background (Fig. 4A). In the grazing section of growth cones, the immunolabeling was also localized close to the edge, near the membranous areas, in addition to being localized at microtubules (Fig. 4B). This suggests that CRMP-2 is present in the vicinity of the plasma membrane of growth cones. For more-precise localization, we employed the freeze-etching immunoreplica method, which illustrates different morphological views, in particular, the membrane cytoskeletal complex (the so-called membrane undercoat). Freeze-etched images showed a few clathrin-coated pits and the cortical actin filaments in the cytoplasmic surface of the apical distal membrane (membrane undercoat) of growth cones. The high-power view of the cytoplasmic surface of the membrane provides evidence that CRMP-2 was localized on clathrin-coated pits (Fig. 4D and E) and actin filaments (Fig. 4G). More than 75% of the clathrin-coated pits showed immunolabeling of CRMP-2 (76.5%; n = 17). Because AP-2, which is a component of clathrin-coated pits, associates with Numb, CRMP-2 is thought to bind to clathrin-coated pits through Numb (56). In contrast, the immunolabeling against phosphorylated CRMP-2 was found only on actin filaments (Fig. 4H) and not on microtubules or clathrin-coated pits (0%, n = 15; Fig. 4C and F). These observations are morphological counterparts of the molecular interaction scheme derived from biochemical experiments on the basis of the idea that CRMP-2 associates with Numb on clathrin-coated pits, microtubules, or actin filaments, whereas phosphorylated CRMP-2 interacts only with actin filaments in growth cones.

We then examined the functional relevance of the relationship between phosphorylation at Thr-555 and CRMP-2 activity in neurons (Fig. 5A). We first characterized two CRMP-2 mutants, one in which the Rho kinase phosphorylation site (Thr-555) is replaced by Asp (CRMP-2 T555D), which is expected to mimic the phosphorylated form (3), and another in

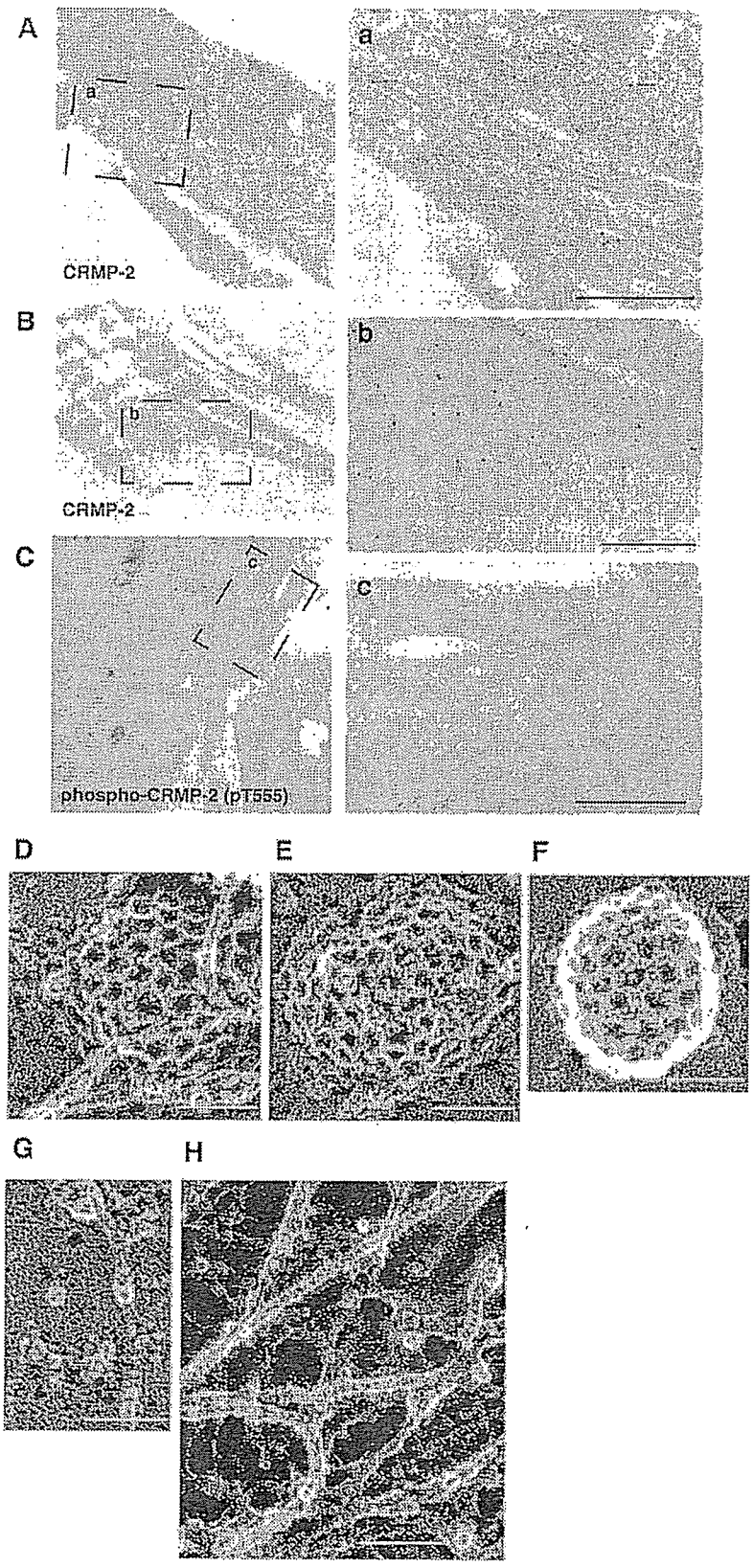
A
a
CRMP-2
B
b
CRMP-2
C
c
phospho-CRMP-2 (pT555)
D
E
F
G
H

which Thr-555 is replaced by Ala (CRMP-2 T555A) and is not phosphorylated by Rho kinase (5). Because ectopic green fluorescent protein (GFP)-tagged CRMP-2 was diffusely distributed, it was difficult to examine the localization of ectopic CRMP-2 in detail at the growth cones. Although we do not know why GFP mutants are located diffusely, this is presumably because neurons express CRMP-2 at levels much higher than other proteins (approximately 1% in total proteins). In contrast, in the cells expressing CRMP-2 at lower levels, we observed the clear colocalization of GFP-CRMP-2 and microtubules. When GFP-CRMP-2 wild type (WT) was expressed in Vero fibroblasts, 72.7% of GFP-tagged CRMP-2-expressing cells ($n = 22$) showed clear localization along the mitotic spindle, as previously described (28, 34) (Fig. 5A). Colocalization of the mutant CRMP-2 T555A with microtubules was also observed in 95.2% of the transfected cells ($n = 21$). However, the mutant CRMP-2 T555D was diffusely distributed, and only 9.5% of GFP-CRMP-2 T555D-expressing cells showed the colocalization with the mitotic spindle ($n = 21$).

Using these mutant constructs, we examined the functional relevance of phosphorylation at Thr-555 and CRMP-2 activity in terms of neurite formation (Fig. 5B). N1E-115 neuroblastoma cells were transfected with CRMP-2 T555D and CRMP-2 T555A. N1E-115 cells have a round morphology in the presence of serum, whereas these cells can differentiate and extend neurites in serum-free medium. In the presence of serum, only about 5% of the cells extended neurites. Under these conditions, expression of CRMP-2 WT increased the numbers of the cells bearing neurites, in contrast to the results seen with control cells expressing GST ($P < 0.01$), as described previously (28) (Fig. 5C). The expression of CRMP-2 T555A increased the percentage of cells bearing neurites ($P < 0.01$), but that of the T555D mutant only slightly increased the percentage ($P > 0.2$). This neurite formation in N1E-115 is known to require the assembly of the microtubules (28). The morphology of neurites induced by the ectopic expression of CRMP-2 WT or T555A was similar to that induced by the serum deprivation, and the neurites had microtubules that were detected with anti-α-tubulin antibody (28) (Fig. 5B).

We next examined the effects of these constructs on axon elongation in DRG neurons. Dissociated DRG neurons were transfected with the plasmids used in Fig. 5B. After transfection, neurons were cultured for 3 days in NGF-deprived medium. Under these conditions, some neurons transfected with control plasmids maintained the long axon. In neurons transfected with CRMP-2 WT, the percentage of the neurons bearing a long axon (>1,300 μm) was increased, in contrast to the control cells expressing GST ($P < 0.01$; Fig. 5D). CRMP-2 T555A had an effect on axon elongation similar to that seen with CRMP-2 WT ($P < 0.01$), but that of T555D was weak ($P < 0.05$). These observations indicate that the dephosphorylated form of CRMP-2 has the ability to promote axon elongation, presumably through the interaction with tubulin and Numb, and that the phosphorylated form of CRMP-2 loses most of ability to support neurite formation in N1E-115 and DRG neurons (Fig. 5C and D). Compared to control results, however, the mutant T555D has at least a weak ability to enhance neurite outgrowth or axon elongation (Fig. 5C and D). Although we do not know why T555D mutants have these positive effects on axon elongation, we think that the mutant T555D may not completely mimic the phosphorylated states, even though it increases the negative charge at the phosphorylation site, as previously reported (15, 25, 47). In fact, 9.5% of GFP-CRMP-2 T555D-expressing cells show the colocalization with mitotic spindles under the conditions in which 72.7% of GFP-CRMP-2 WT colocalized with spindles (Fig. 5A). Thus, it appears that the T555D mutant still keeps some activity to interact with tubulin and/or microtubules, thereby promoting neurite elongation. Alternatively, this implies the existence of other mechanisms that enhance neurite elongation, which are regulated independently of phosphorylation by Rho kinase at Thr-555.

As we reported previously, CRMP-2 is phosphorylated by Rho kinase during LPA-induced growth cone collapse (5). However, its physiological role in axon guidance is still unknown. Thus, we examined the physiological role of the phosphorylation of CRMP-2 by Rho kinase in growth cone collapse induced by repulsive guidance cues (Fig. 6). As some groups have reported, several repulsive axon guidance cues stimulate Rho/Rho kinase signaling to induce growth cone collapse (74). Among them, ephrin-A5 induces the phosphorylation of MLC through Rho kinase (71). We then examined whether ephrin-A5 induces CRMP-2 phosphorylation by Rho kinase at Thr-555. DRG neurons cultured for 24 h were serum starved for 4 h and then stimulated by ephrin-A5 for 3, 10, and 30 min; these stimuli induced growth cone collapse. The addition of ephrin-A5 induced rapid phosphorylation of endogenous CRMP-2 at Thr-555 (Fig. 6A). The phosphorylation increased up to about sixfold more than the basal level during the first 3 min (Fig. 6A and B). To examine whether ephrin-A5-induced phosphorylation of CRMP-2 at Thr-555 was mediated by Rho kinase, DRG neurons were stimulated by ephrin-A5 in the presence of Rho kinase inhibitor (Y-27632 or HA1077) for 1 h (69). Y-27632 and HA1077 inhibited the ephrin-A5-induced phosphorylation of CRMP-2 (Fig. 6A and B). These results indicate that CRMP-2 is phosphorylated at Thr-555 by Rho kinase during ephrin-A5-induced growth cone collapse of DRG neurons, as well during as during that induced by LPA, as reported previously (5). We then examined the localization of phosphorylated CRMP-2 after the stimulation with ephrin-

FIG. 4. Electron microscopic immunocytochemical localization of CRMP-2 in chick DRG growth cones. (A to C) Horizontal section of central area of growth cones. Enlarged images from insets a to c in panels A to C are shown in panels a to c. In panels a and b, red arrows indicate the immunolabeling of CRMP-2. Thin lines are microtubule filaments. (B) Grazing section of growth cones. Red arrows indicate the immunolabeling of CRMP-2 close to the plasma membrane. (C) Immunolabeling with anti-phospho-CRMP-2 was not observed. Bars (panels a to c), 500 nm. (D to H) High-power view of the sample prepared by freeze-etching immunoreplica methods (negative images are shown for clarity). Immunocolloidal gold is shown as white dots. Red arrows indicate the immunolabeling of CRMP-2 on clathrin-coated pits (D and E) and on actin filaments (G) or of phosphorylated CRMP-2 on actin filaments (H). Immunolabeling with anti-phospho-CRMP-2 antibody was not observed on clathrin-coated pits (F). Bar (D to H), 50 nm.

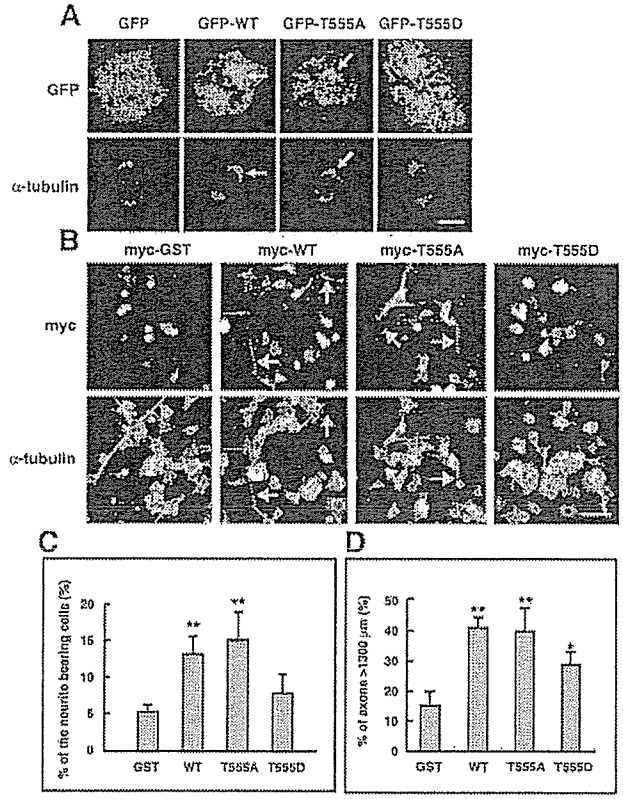

FIG. 5. Effects of CRMP-2 mutants on neurite formation in N1E-115 cells and DRG neurons. (A) Localization of GFP-tagged CRMP-2 and CRMP-2 mutants T555A and T555D. Vero cells were transfected with pEGFP-CRMP-2 WT, T555A, or T555D and cultured for 36 h. Transfected cells were fixed and stained with anti-α-tubulin antibody. Arrows indicate the colocalization of GFP-fused protein with microtubules. Bar, 10 μm. (B) The effect of overexpression of CRMP-2 WT, T555A, and T555D on process formation in N1E-115 cells. N1E-115 cells were transfected with myc-GST (as a negative control), CRMP-2 WT, T555A, or T555D. Twenty-four hours after transfection, the cells were cultured in serum-containing medium for 24 h. Transfected cells were fixed and doubly stained by anti-myc antibody (top panels) and anti-α-tubulin antibody (bottom panels). Arrows indicate the processes induced by CRMP-2 constructs. Bar, 40 μm. (C) The percentage of cells bearing neurites (length > 20 μm) in transfected cells. Fifty randomly selected transfected neurons were quantified for each construct. The values shown are means ± standard errors of triplicate experiments. **, significantly different from the cells expressing GST as analyzed by Student's *t* test ($P < 0.01$). (D) The percentage of cells bearing axons (length > 1,300 μm) in DRG neuron-transfected cells. DRG neurons were transfected with the plasmids indicated in panel B. After transfection, the neurons were cultured in the NGF-deprived medium for 3 days. Transfected neurons were fixed and doubly stained by anti-myc antibody and anti-neurofilament antibody. The percentage of neurons bearing axons with length > 1,300 μm versus the total number of neurons bearing axons was analyzed. Fifty randomly selected transfected neurons were quantified for each construct. The values shown are means ± standard errors of triplicate experiments. **, significantly different from the cells expressing GST as analyzed by Student's *t* test ($P < 0.01$); *, $P < 0.05$.

A5. Because ephrin-A5 treatment makes the growth cone collapse, the relative amount of increased phosphorylation of CRMP-2 could not be measured in spreading growth cones (data not shown). However, higher immunolabeling of phosphorylated CRMP-2 was observed in collapsed growth cones (Fig. 6C and D). Y-27632 prevented the growth cone collapse, as reported previously (71), and inhibited an increase of phosphorylated CRMP-2 levels at the tips of axons (data not shown). Staining by the phospho-CRMP-2 antibody was visible as dot-like structures in both the growth cone and axon shaft compared to the results seen with CRMP-2 antibody. The nature of this dot-like structure has not been elucidated.

To examine the role of CRMP-2 phosphorylation in growth cone morphology, we expressed the CRMP-2 mutants T555A and T555D in DRG neurons. The expression of CRMP-2 WT had no effect on ephrin-A5-induced growth cone collapse compared to the control results, whereas the expression of the mutant CRMP-2 T555A partially inhibited ephrin-A5-induced growth cone collapse ($P < 0.05$; Fig. 6C, bottom panel). These results suggest that phosphorylation of CRMP-2 at Thr-555 is partially involved in ephrin-A5-induced growth cone collapse. Of note, the effect of the T555A mutant is not complete, because the endogenous CRMP-2 expression level is relatively high in DRG neurons (39), and the nonphosphorylated form of CRMP-2 may not completely replace endogenous CRMP-2. In addition, a lot of substrates of Rho kinase have been reported and are expected to participate partially in growth cone collapse, as previously reported (71). Finally, it should be noted that the expression of CRMP-2 T555D increased the number of collapsed growth cones and slightly inhibited ephrin-A5-induced growth cone collapse. Although the exact mode of action of CRMP-2 T555D is not known, this mutant may mimic phosphorylated CRMP-2 and induce growth cone collapse while partially inhibiting Rho kinase activity in a manner competitive with endogenous CRMP-2.

DISCUSSION

CRMP-2 was first reported as a mediator of Sema3A-induced growth cone collapse (31). However, the molecular mechanisms involving CRMP-2 in growth cone collapse have not been elucidated. We previously reported that Rho kinase phosphorylates CRMP-2 at Thr-555 during LPA-induced, but not Sema3A-induced, growth cone collapse in DRG neurons (5) and that overexpression of CRMP-2 in hippocampal neurons enhances axon formation by its association with tubulin heterodimer and Numb (28, 34, 39, 56). CRMP-2 functions as a carrier of tubulin heterodimers, which delivers tubulin dimers to the assembly plus ends of nucleating sites or growing microtubules (28). CRMP-2 associates with Numb and regulates L1 endocytosis at axonal growth cones in hippocampal neurons (56). Although these reports revealed that CRMP-2 functions in axon elongation, the molecular mechanisms involving CRMP-2 and its interacting molecules in growth cone collapse remain unresolved. And we also reported the involvement of phosphorylation at Thr-514 by GSK-3β in neuronal polarity and that Thr-522 was phosphorylated by Cdk5 downstream of Sema3A (68, 73) but have not investigated the meaning of these phosphorylation events with respect to the growth cone collapse. In the present study, we found that phosphorylation by Rho kinase inhibits the ability of CRMP-2 to bind tubulin and Numb. These interactions are necessary for growth cone advance and axon growth. Therefore, we suggest that ephrin-A5 stimulation dissociates CRMP-2 from interacting

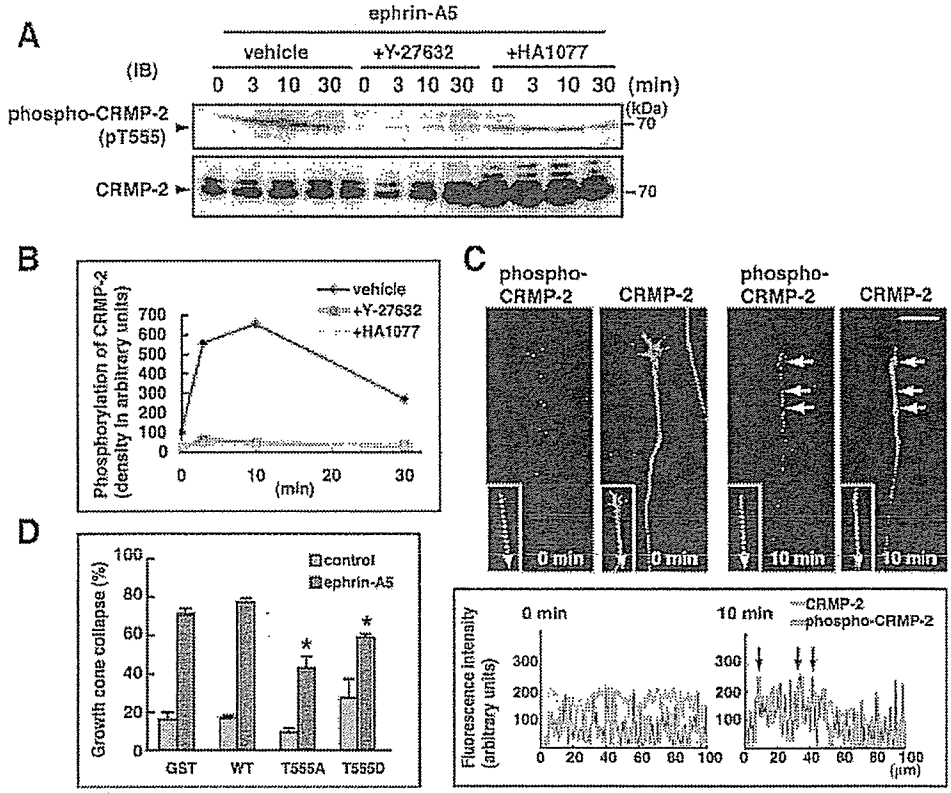

FIG. 6. Ephrin-A5-induced CRMP-2 phosphorylation. (A) DRG neurons were serum starved for 4 h and stimulated by 1 μg/ml ephrin-A5 with or without pretreatment with 10 μM Rho kinase inhibitor (Y-27632 or HA1077) for 0, 3, 10, and 30 min. The cell lysate was resolved by SDS-PAGE and immunoblotted (IB) with the indicated antibodies. The multiple bands of CRMP-2 represent differentially phosphorylated forms (33). Arrowheads indicate the intact protein of CRMP-2. The band corresponding to the phosphorylated form by Rho kinase was detected at the same position as the main band detected by anti-CRMP-2 antibody. The results are representative of three independent experiments. (B) The relative levels resulting from CRMP-2 phosphorylation were calculated, with the level obtained with untreated control cells defined as 100 units. (C) The localization of phosphorylated CRMP-2 before and after stimulation with ephrin-A5 in DRG neurons. DRG neurons were serum starved for 4 h and stimulated by 1 μg/ml ephrin-A5. Before stimulation and 10 min after stimulation with ephrin-A5, cells were fixed and immunostained with anti-phospho-CRMP-2 antibody (red) and anti-CRMP-2 antibody (green). Arrows indicate the collapsed growth cone and axonal shaft, which was intensely stained by anti-phospho-CRMP-2 antibody. Bar, 20 μm. The fluorescence intensities of CRMP-2 (green) and phospho-CRMP-2 (red) in the dotted lines are shown in the graphs (bottom panel). Arrows indicate the same positions as the areas indicated by arrows in the images (upper panels). (D) Effects of CRMP-2 mutants T555A and T555D on ephrin-A5-induced growth cone collapse. DRG neurons transfected with myc-GST, CRMP-2 WT, T555A, or T555D were stimulated with ephrin-A5 for 30 min. Then the population of collapsed growth cones expressing introduced constructs was calculated. Thirty randomly selected transfected neurons were quantified for each construct. The values shown are means ± standard errors of triplicate experiments. *, significantly different from the growth cones expressing GST as analyzed by Student's t test ($P < 0.05$).

molecules by phosphorylation and enhances growth cone collapse.

In previous reports, we showed that CRMP-2 enhances microtubule assembly and, thereby, axon formation (28). And here we report that the phosphorylation by Rho kinase prevents the association with tubulin dimer-microtubules. This regulation of CRMP-2 activity seems to cause the reduction of microtubule assembly. The plus ends of microtubules in growth cones exhibit a property termed dynamic instability, wherein they cycle through periods of growth and shrinkage (6, 27, 53, 65). The increase of microtubule assembly is required for the growth cone advance (27, 28). In fact, some groups showed that the polymerization and capturing of microtubules in one direction and the shrinkage of microtubules in the other direction are early steps in guidance of axonal growth cones, suggesting that the regulation of microtubule dynamic instability is closely related to the morphological changes of growth cones (11, 60, 66, 76). Therefore, the enhancement of microtubule assembly by CRMP-2 is critical for the growth cone dynamics. The canceling of the interaction of CRMP-2 and tubulin dimer and/or microtubules by phosphorylation is thought to prevent the proper microtubule formation. Taken together, these data indicate that the negative regulation of CRMP-2 activity appears to disrupt the normal microtubule dynamics, followed by the collapse of growth cone morphology.

Knockdown of CRMP-2 in hippocampal neurons inhibits Numb-mediated L1 endocytosis and axon growth (56). Here we report that phosphorylated CRMP-2 could not associate with Numb. Thus, it is possible that CRMP-2 phosphorylation also inhibits Numb-mediated L1 endocytosis. However, two groups have reported that growth cone collapse triggered by Sema3A or ephrins was accompanied by enhanced endocytosis (26, 41); they observed the fluorescence-labeled dextran uptake or reorganization of signaling molecules neuropilin 1

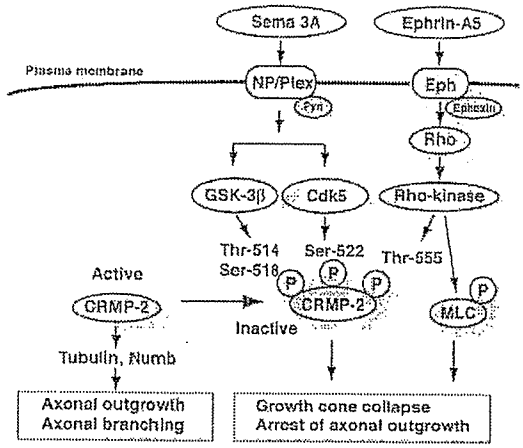

FIG. 7. Model schema for the phosphorylation of CRMP-2 by Rho kinase, Cdk5, and GSK-3β. Sema3A is thought to activate Cdk5 and GSK-3β. These activations cause phosphorylation at Ser-522, Ser-518, and Thr-514. Ephrin-A5 stimulation activates the Rho/Rho kinase signaling pathway and subsequently induces the phosphorylation of CRMP-2 at Thr-555 by Rho kinase. The binding activity of CRMP-2 to tubulin is decreased by the phosphorylation by Cdk5, GSK-3β, and Rho kinase. Nonphosphorylated CRMP-2 binds to tubulin heterodimers to promote microtubule assembly or Numb-mediated endocytosis, thereby enhancing axon elongation and branching. In contrast, the phosphorylated form cannot associate with interacting molecules and loses the positive effect on axon elongation, thereby causing arrest of axon growth and growth cone collapse.

(NP1), plexin, and Rac in response to guidance cues. In a reconstituted Sema3A signaling system in COS-7 cells expressing the receptor components NP1 and plexin A1, CRMP and plexin A1 form a physical complex and CRMP accelerates Sema3A-induced cell contraction (17). In contrast, NGF signaling increases clathrin-coated membrane formation and clathrin-mediated membrane trafficking, as revealed by the increased endocytosis of transferrin (7). Judging from these reports, endocytosis appears to be selectively regulated for axon outgrowth and growth cone collapse. L1 and L1 recycling are crucial for axon elongation and growth cone motility (43). Inactivation of CRMP-2 may be required for the selective inhibition of cell adhesion molecules to prevent the growth cone dynamics. Although the exact mechanisms causing growth cone collapse need additional study, our results imply that ephrin-A5-induced growth cone collapse is enhanced by the CRMP-2 phosphorylation through the inhibition of Numb-mediated endocytosis.

CRMP-2 is implicated in Sema3A-induced growth cone collapse (31). The phosphorylation of CRMP-2 at Thr-555 by Rho kinase was observed during LPA-induced growth cone collapse but not during Sema3A-induced collapse (5). In retinal ganglion cells, ephrin-A5-induced growth cone collapse is mediated by Rho kinase (13, 71). In the present study, we found that Rho kinase phosphorylates CRMP-2 at Thr-555 in response to ephrin-A5. It has been reported that activation of Fyn, Cdk5, and GSK-3β is involved in Sema3A signaling (22, 62) (Fig. 7). Activated Cdk5 phosphorylates Tau and causes microtubule reorganization induced by Sema3A (62). Recently, our group and several other groups have reported that CRMP-2 is phosphorylated by Cdk5, dual tyrosine-regulated kinase (DYRK), and GSK-3β (10, 14, 73). Cdk5 and DYRK phosphorylate CRMP-2 at Ser-522, and this phosphorylation site acts as a priming site for subsequent GSK-3β phosphorylation at Ser-518 and Thr-514. Here, we found that the phosphorylation of CRMP-2 by Cdk5 and GSK-3β cancels the binding activity to tubulin and Numb. Thus, both signaling pathways downstream of Sema3A and ephrin-A5 as well as LPA seem to terminate in the same molecule, CRMP-2, through activation by different kinases, followed by microtubule reorganization (Fig. 7). On the other hand, we reported that neurotropic factors BDNF and NT-3, but not NGF, inhibit the phosphorylation of CRMP-2 via PI 3-kinase and Akt in hippocampal neurons (73). These growth factors are known to prevent growth cone collapse in response to the repulsive guidance cues (20, 67). Thus, it appears that attractive and repulsive extracellular cues regulate the balance of phosphorylation and dephosphorylation in CRMP-2, thereby managing microtubule formation and endocytosis. The function of CRMP-2 would be dramatically regulated by several kinds of kinases in response to extracellular stimulation.

Rho kinase has multiple substrates regulating the dynamics of the actin filament (35, 42). Rho kinase regulates the phosphorylation of MLC, resulting in actomyosin contractility, which is observed during ephrin-A5-induced growth cone collapse (71). We recently found that Rho kinase phosphorylates the microtubule-associated proteins (MAPs) Tau and MAP-2 (3, 4). This phosphorylation dissociates MAPs from microtubule filaments in neurons. In fact, in this study the mutant that mimicked CRMP-2 phosphorylated by Rho kinase could not inhibit the ephrin-A5-induced growth cone collapse completely, suggesting that Rho kinase is likely to phosphorylate multiple substrates, including MLC and MAPs, to achieve growth cone collapse. Because nonphosphorylated CRMP-2 can enhance the assembly of microtubules, we speculate that phosphorylated CRMP-2 may lose the ability to drive the microtubule formation, thus causing the destabilization of microtubule formation, in association with phosphorylated MAPs.

We found actin to be a CRMP-2-interacting protein. Both phosphorylated and nonphosphorylated forms of CRMP-2 bound to actin in vitro, and CRMP-2 was detected on actin filaments in DRG neuron growth cones. We examined whether CRMP-2 associates with actin monomer in vitro by use of purified actin monomers and recombinant CRMP-2 proteins, but a direct association was not observed. In another study, we have recently found that CRMP-2 interacts with Specifically Rac1-Associated protein (Sra-1/CYFIP1) (43a), which directly interacts with actin filaments (45). Thus, CRMP-2 may associate with actin filaments through Sra-1 in growth cones. In this study, Rho kinase-induced phosphorylation of CRMP-2 had no effect on the actin binding ability of CRMP-2. CRMP-2 is a highly conserved phosphoprotein, and its phosphorylation states alter upon NGF-induced neuronal differentiation or in the formation of degenerating neurites in the brains of patients with Alzheimer's disease (12, 33). These findings raise the possibility that other kinases up- or down-regulate CRMP-2 activity and mediate actin reorganization in the Rho family GTPase-mediated signal cascade. Further studies characterizing the protein kinases may shed some light on other functions of CRMP-2.

ACKNOWLEDGMENTS

We thank Y. Gu, Y. Ihara, E. Mekada, T. Kato, and H. Tanaka for their kind gifts of materials. We also thank T. Nishimura and N. Mishima Yoshimura (Nagoya University) for helpful discussion and preparing some materials and T. Ishii for secretarial and technical assistance.

This work was supported by Grants-in-Aid for scientific research from the Ministry of Education, Culture, Sports, Science and Technology of Japan, a Grant-in-Aid for Creative Scientific Research from the Ministry of Education, Culture, Sports, Science and Technology of Japan (MEXT), Special Coordination Funds for Promoting Science and Technology (SCFPST), National Institute of Biomedical Innovation, Research Fellowships of the Japan Society for the Promotion of Science for Young Scientists (JSPS), the 21st Century Centre of Excellence (COE) Program from MEXT, and a Research Grant (15A-2) for Nervous and Mental Disorders from the Ministry of Health, Labor and Welfare.

REFERENCES

1. **Amano, M., K. Chihara, N. Nakamura, Y. Fukata, T. Yano, M. Shibata, M. Ikebe, and K. Kaibuchi.** 1998. Myosin II activation promotes neurite retraction during the action of Rho and Rho-kinase. Genes Cells 3:177–188.
2. **Amano, M., M. Ito, K. Kimura, Y. Fukata, K. Chihara, T. Nakano, Y. Matsuura, and K. Kaibuchi.** 1996. Phosphorylation and activation of myosin by Rho-associated kinase (Rho-kinase). J. Biol. Chem. 271:20246–20249.
3. **Amano, M., T. Kaneko, A. Maeda, M. Nakayama, M. Ito, T. Yamauchi, H. Goto, Y. Fukata, N. Oshiro, A. Shinohara, A. Iwamatsu, and K. Kaibuchi.** 2003. Identification of Tau and MAP2 as novel substrates of Rho-kinase and myosin phosphatase. J. Neurochem. 87:780–790.
4. **Amano, M., Y. Fukata, and K. Kaibuchi.** 2000. Regulation and functions of Rho-associated kinase. Exp. Cell Res. 261:44–51.
5. **Arimura, N., N. Inagaki, K. Chihara, C. Menager, N. Nakamura, M. Amano, A. Iwamatsu, Y. Goshima, and K. Kaibuchi.** 2000. Phosphorylation of collapsin response mediator protein-2 by Rho-kinase. Evidence for two separate signaling pathways for growth cone collapse. J. Biol. Chem. 275:23973–23980.
6. **Baas, P. W., M. M. Black, and G. A. Banker.** 1989. Changes in microtubule polarity orientation during the development of hippocampal neurons in culture. J. Cell Biol. 109:3085–3094.
7. **Beattie, E. C., C. L. Howe, A. Wilde, F. M. Brodsky, and W. C. Mobley.** 2000. NGF signals through TrkA to increase clathrin at the plasma membrane and enhance clathrin-mediated membrane trafficking. J. Neurosci. 20:7325–7333.
8. **Berninger, B., D. E. Garcia, N. Inagaki, C. Hahnel, and D. Lindholm.** 1993. BDNF and NT-3 induce intracellular $Ca2^+$ elevation in hippocampal neurones. Neuroreport 4:1303–1306.
9. **Bito, H., T. Furuyashiki, H. Ishihara, Y. Shibasaki, K. Ohashi, K. Mizuno, M. Maekawa, T. Ishizaki, and S. Narumiya.** 2000. A critical role for a Rho-associated kinase, p160ROCK, in determining axon outgrowth in mammalian CNS neurons. Neuron 26:431–441.
10. **Brown, M., T. Jacobs, B. Eickholt, G. Ferrari, M. Teo, C. Monfries, R. Z. Qi, T. Leung, L. Lim, and C. Hall.** 2004. Alpha2-chimaerin, cyclin-dependent kinase 5/p35, and its target collapsin response mediator protein-2 are essential components in semaphorin 3A-induced growth-cone collapse. J. Neurosci. 24:8994–9004.
11. **Buck, K. B., and J. Q. Zheng.** 2002. Growth cone turning induced by direct local modification of microtubule dynamics. J. Neurosci. 22:9358–9367.
12. **Byk, T., S. Ozon, and A. Sobel.** 1998. The Ulip family phosphoproteins—common and specific properties. Eur. J. Biochem. 254:14–24.
13. **Cheng, Q., Y. Sasaki, M. Shoji, Y. Sugiyama, H. Tanaka, T. Nakayama, N. Mizuki, F. Nakamura, K. Takei, and Y. Goshima.** 2003. Cdk5/p35 and Rho-kinase mediate ephrin-A5-induced signaling in retinal ganglion cells. Mol. Cell. Neurosci. 24:632–645.
14. **Cole, A. R., A. Knebel, N. A. Morrice, L. S. Robertson, A. J. Irving, C. N. Connolly, and C. Sutherland.** 2004. GSK-3 phosphorylation of the Alzheimer epitope within collapsin response mediator proteins regulates axon elongation in primary neurons. J. Biol. Chem. 279:50176–50180.
15. **Dean, A. M., and D. E. Koshland, Jr.** 1990. Electrostatic and steric contributions to regulation at the active site of isocitrate dehydrogenase. Science 249:1044–1046.
16. **Dent, E. W., and F. B. Gertler.** 2003. Cytoskeletal dynamics and transport in growth cone motility and axon guidance. Neuron 40:209–227.
17. **Deo, R. C., E. F. Schmidt, A. Elhabazi, H. Togashi, S. K. Burley, and S. M. Strittmatter.** 2004. Structural bases for CRMP function in plexin-dependent semaphorin3A signaling. EMBO J. 23:9–22.
18. **Diefenbach, T. J., P. B. Guthrie, H. Stier, B. Billups, and S. B. Kater.** 1999. Membrane recycling in the neuronal growth cone revealed by FM1-43 labeling. J. Neurosci. 19:9436–9444.
19. **Donoghue, M. J., R. M. Lewis, J. P. Merlie, and J. R. Sanes.** 1996. The Eph kinase ligand AL-1 is expressed by rostral muscles and inhibits outgrowth from caudal neurons. Mol. Cell. Neurosci. 8:185–198.
20. **Dontchev, V. D., and P. C. Letourneau.** 2002. Nerve growth factor and semaphorin 3A signaling pathways interact in regulating sensory neuronal growth cone motility. J. Neurosci. 22:6659–6669.
21. **Drescher, U., F. Bonhoeffer, and B. K. Muller.** 1997. The Eph family in retinal axon guidance. Curr. Opin. Neurobiol. 7:75–80.
22. **Eickholt, B. J., F. S. Walsh, and P. Doherty.** 2002. An inactive pool of GSK-3 at the leading edge of growth cones is implicated in semaphorin 3A signaling. J. Cell Biol. 157:211–217.
23. **Fan, J., and J. A. Raper.** 1995. Localized collapsing cues can steer growth cones without inducing their full collapse. Neuron 14:263–274.
24. **Flanagan, J. G., and P. Vanderhaeghen.** 1998. The ephrins and Eph receptors in neural development. Annu. Rev. Neurosci. 21:309–345.
25. **Fong, Y. L., W. L. Taylor, A. R. Means, and T. R. Soderling.** 1989. Studies of the regulatory mechanism of $Ca2^+$/calmodulin-dependent protein kinase II. Mutation of threonine 286 to alanine and aspartate. J. Biol. Chem. 264: 16759–16763.
26. **Fournier, A. E., F. Nakamura, S. Kawamoto, Y. Goshima, R. G. Kalb, and S. M. Strittmatter.** 2000. Semaphorin3A enhances endocytosis at sites of receptor-F-actin colocalization during growth cone collapse. J. Cell Biol. 149:411–422.
27. **Fukata, M., M. Nakagawa, and K. Kaibuchi.** 2003. Roles of Rho-family GTPases in cell polarisation and directional migration. Curr. Opin. Cell Biol. 15:590–597.
28. **Fukata, Y., T. J. Itoh, T. Kimura, C. Menager, T. Nishimura, T. Shiromizu, H. Watanabe, N. Inagaki, A. Iwamatsu, H. Hotani, and K. Kaibuchi.** 2002. CRMP-2 binds to tubulin heterodimers to promote microtubule assembly. Nat. Cell Biol. 4:583–591.
29. **Ganju, P., K. Shigemoto, J. Brennan, A. Entwistle, and A. D. Reith.** 1994. The Eck receptor tyrosine kinase is implicated in pattern formation during gastrulation, hindbrain segmentation and limb development. Oncogene 9:1613–1624.
30. **Goshima, Y., T. Kawakami, H. Hori, Y. Sugiyama, S. Takasawa, Y. Hashimoto, M. Kagoshima-Maezono, T. Takenaka, Y. Misu, and S. M. Strittmatter.** 1997. A novel action of collapsin: collapsin-1 increases antero- and retrograde axoplasmic transport independently of growth cone collapse. J. Neurobiol. 33:316–328.
31. **Goshima, Y., F. Nakamura, P. Strittmatter, and S. M. Strittmatter.** 1995. Collapsin-induced growth cone collapse mediated by an intracellular protein related to UNC-33. Nature 376:509–514.
32. **Grunwald, I. C., and R. Klein.** 2002. Axon guidance: receptor complexes and signaling mechanisms. Curr. Opin. Neurobiol. 12:250–259.
33. **Gu, Y., N. Hamajima, and Y. Ihara.** 2000. Neurofibrillary tangle-associated collapsin response mediator protein-2 (CRMP-2) is highly phosphorylated on Thr-509, Ser-518, and Ser-522. Biochemistry 39:4267–4275.
34. **Gu, Y., and Y. Ihara.** 2000. Evidence that collapsin response mediator protein-2 is involved in the dynamics of microtubules. J. Biol. Chem. 275:17917–17920.
35. **Hall, A.** 1998. Rho GTPases and the actin cytoskeleton. Science 279:509–514.
36. **Hall, A., and C. D. Nobes.** 2000. Rho GTPases: molecular switches that control the organization and dynamics of the actin cytoskeleton. Philos. Trans. R. Soc. Lond. B Biol. Sci. 355:965–970.
37. **Hedgecock, E. M., J. G. Culotti, J. N. Thomson, and L. A. Perkins.** 1985. Axonal guidance mutants of *Caenorhabditis elegans* identified by filling sensory neurons with fluorescein dyes. Dev. Biol. 111:158–170.
38. **Hirose, M., T. Ishizaki, N. Watanabe, M. Uehata, O. Kranenburg, W. H. Moolenaar, F. Matsumura, M. Maekawa, H. Bito, and S. Narumiya.** 1998. Molecular dissection of the Rho-associated protein kinase (p160ROCK)-regulated neurite remodeling in neuroblastoma N1E-115 cells. J. Cell Biol. 141:1625–1636.
39. **Inagaki, N., K. Chihara, N. Arimura, C. Menager, Y. Kawano, N. Matsuo, T. Nishimura, M. Amano, and K. Kaibuchi.** 2001. CRMP-2 induces axons in cultured hippocampal neurons. Nat. Neurosci. 4:781–782.
40. **Ishizaki, T., M. Maekawa, K. Fujisawa, K. Okawa, A. Iwamatsu, A. Fujita, N. Watanabe, Y. Saito, A. Kakizuka, N. Morii, and S. Narumiya.** 1996. The small GTP-binding protein Rho binds to and activates a 160 kDa Ser/Thr protein kinase homologous to myotonic dystrophy kinase. EMBO J. 15: 1885–1893.
41. **Jurney, W. M., G. Gallo, P. C. Letourneau, and S. C. McLoon.** 2002. Rac1-mediated endocytosis during ephrin-A2- and semaphorin 3A-induced growth cone collapse. J. Neurosci. 22:6019–6028.
42. **Kaibuchi, K., S. Kuroda, and M. Amano.** 1999. Regulation of the cytoskeleton and cell adhesion by the Rho family GTPases in mammalian cells. Annu. Rev. Biochem. 68:459–486.
43. **Kamiguchi, H., and V. Lemmon.** 2000. Recycling of the cell adhesion molecule L1 in axonal growth cones. J. Neurosci. 20:3676–3686.

43a. **Kawano, Y., T. Yoshimura, D. Tsuboi, S. Kawabata, T. Kaneko-Kawano, H. Shirataki, T. Takenawa, and K. Kaibuchi.** 2005. CRMP-2 is involved in kinesin-1-dependent transport of the Sra-1/WAVE1 complex and axon formation. Mol. Cell. Biol. 25:9920–9935.

44. Knoll, B., and U. Drescher. 2004. Src family kinases are involved in EphA receptor-mediated retinal axon guidance. J. Neurosci. 24:6248–6257.
45. Kobayashi, K., S. Kuroda, M. Fukata, T. Nakamura, T. Nagase, N. Nomura, Y. Matsuura, N. Yoshida-Kubomura, A. Iwamatsu, and K. Kaibuchi. 1998. p140Sra-1 (specifically Rac1-associated protein) is a novel specific target for Rac1 small GTPase. J. Biol. Chem. 273:291–295.
46. Kullander, K., and R. Klein. 2002. Mechanisms and functions of Eph and ephrin signalling. Nat. Rev. Mol. Cell Biol. 3:475–486.
47. Kurland, I. J., M. R. el-Maghrabi, J. J. Correia, and S. J. Pilkis. 1992. Rat liver 6-phosphofructo-2-kinase/fructose-2,6-bisphosphatase. Properties of phospho- and dephospho- forms and of two mutants in which Ser32 has been changed by site-directed mutagenesis. J. Biol. Chem. 267:4416–4423.
48. Lai, K. O., F. C. Ip, and N. Y. Ip. 1999. Identification and characterization of splice variants of ephrin-A3 and ephrin-A5. FEBS Lett. 458:265–269.
49. Li, W., R. K. Herman, and J. E. Shaw. 1992. Analysis of the *Caenorhabditis elegans* axonal guidance and outgrowth gene unc-33. Genetics 132:675–689.
50. Liu, X., K. Seno, Y. Nishizawa, F. Hayashi, A. Yamazaki, H. Matsumoto, T. Wakabayashi, and J. Usukura. 1994. Ultrastructural localization of retinal guanylate cyclase in human and monkey retinas. Exp. Eye Res. 59:761–768.
51. Mack, T. G., M. P. Koester, and G. E. Pollerberg. 2000. The microtubule-associated protein MAP1B is involved in local stabilization of turning growth cones. Mol. Cell. Neurosci. 15:51–65.
52. Matsuura, Y., R. D. Possee, H. A. Overton, and D. H. Bishop. 1987. Baculovirus expression vectors: the requirements for high level expression of proteins, including glycoproteins. J. Gen. Virol. 68(Pt. 5):1233–1250.
53. Mitchison, T., and M. Kirschner. 1984. Dynamic instability of microtubule growth. Nature 312:237–242.
54. Mitsui, N., R. Inatome, S. Takahashi, Y. Goshima, H. Yamamura, and S. Yanagi. 2002. Involvement of Fes/Fps tyrosine kinase in semaphorin3A signaling. EMBO J. 21:3274–3285.
55. Mueller, B. K. 1999. Growth cone guidance: first steps towards a deeper understanding. Annu. Rev. Neurosci. 22:351–388.
56. Nishimura, T., Y. Fukata, K. Kato, T. Yamaguchi, Y. Matsuura, H. Kamiguchi, and K. Kaibuchi. 2003. CRMP-2 regulates polarized Numb-mediated endocytosis for axon growth. Nat. Cell Biol. 5:819–826.
57. Ohta, K., H. Iwamasa, U. Drescher, H. Terasaki, and H. Tanaka. 1997. The inhibitory effect on neurite outgrowth of motoneurons exerted by the ligands ELF-1 and RAGS. Mech. Dev. 64:127–135.
58. Quinn, C. C., E. Chen, T. G. Kinjo, G. Kelly, A. W. Bell, R. C. Elliott, P. S. McPherson, and S. Hockfield. 2003. TUC-4b, a novel TUC family variant, regulates neurite outgrowth and associates with vesicles in the growth cone. J. Neurosci. 23:2815–2823.
59. Raper, J. A., and J. P. Kapfhammer. 1990. The enrichment of a neuronal growth cone collapsing activity from embryonic chick brain. Neuron 4:21–29.
60. Sabry, J. H., T. P. O'Connor, L. Evans, A. Toroian-Raymond, M. Kirschner, and D. Bentley. 1991. Microtubule behavior during guidance of pioneer neuron growth cones in situ. J. Cell Biol. 115:381–395.
61. Sahin, M., P. L. Greer, M. Z. Lin, H. Poucher, J. Eberhart, S. Schmidt, T. M. Wright, S. M. Shamah, S. O'Connell, C. W. Cowan, L. Hu, J. L. Goldberg, A. Debant, G. Corfas, C. E. Krull, and M. E. Greenberg. 2005. Eph-dependent tyrosine phosphorylation of ephexin1 modulates growth cone collapse. Neuron 46:191–204.
62. Sasaki, Y., C. Cheng, Y. Uchida, O. Nakajima, T. Ohshima, T. Yagi, M. Taniguchi, T. Nakayama, R. Kishida, Y. Kudo, S. Ohno, F. Nakamura, and Y. Goshima. 2002. Fyn and Cdk5 mediate semaphorin-3A signaling, which is involved in regulation of dendrite orientation in cerebral cortex. Neuron 35:907–920.
63. Shamah, S. M., M. Z. Lin, J. L. Goldberg, S. Estrach, M. Sahin, L. Hu, M. Bazalakova, R. L. Neve, G. Corfas, A. Debant, and M. E. Greenberg. 2001. EphA receptors regulate growth cone dynamics through the novel guanine nucleotide exchange factor ephexin. Cell 105:233–244.
64. Song, H. J., and M. M. Poo. 1999. Signal transduction underlying growth cone guidance by diffusible factors. Curr. Opin. Neurobiol. 9:355–363.
65. Tanaka, E., T. Ho, and M. W. Kirschner. 1995. The role of microtubule dynamics in growth cone motility and axonal growth. J. Cell Biol. 128:139–155.
66. Tanaka, E., and M. W. Kirschner. 1995. The role of microtubules in growth cone turning at substrate boundaries. J. Cell Biol. 128:127–137.
67. Tuttle, R., and D. D. O'Leary. 1998. Neurotrophins rapidly modulate growth cone response to the axon guidance molecule, collapsin-1. Mol. Cell. Neurosci. 11:1–8.
68. Uchida, Y., T. Ohshima, Y. Sasaki, H. Suzuki, S. Yanai, N. Yamashita, F. Nakamura, K. Takei, Y. Ihara, K. Mikoshiba, P. Kolattukudy, J. Honnorat, and Y. Goshima. 2005. Semaphorin3A signalling is mediated via sequential Cdk5 and GSK3beta phosphorylation of CRMP2: implication of common phosphorylating mechanism underlying axon guidance and Alzheimer's disease. Genes Cells 10:165–179.
69. Uehata, M., T. Ishizaki, H. Satoh, T. Ono, T. Kawahara, T. Morishita, H. Tamakawa, K. Yamagami, J. Inui, M. Maekawa, and S. Narumiya. 1997. Calcium sensitization of smooth muscle mediated by a Rho-associated protein kinase in hypertension. Nature 389:990–994.
70. Usukura, J., and D. Bok. 1987. Changes in the localization and content of opsin during retinal development in the rds mutant mouse: immunocytochemistry and immunoassay. Exp. Eye Res. 45:501–515.
71. Wahl, S., H. Barth, T. Ciossek, K. Aktories, and B. K. Mueller. 2000. Ephrin-A5 induces collapse of growth cones by activating Rho and Rho kinase. J. Cell Biol. 149:263–270.
72. Wilkinson, D. G. 2000. Eph receptors and ephrins: regulators of guidance and assembly. Int. Rev. Cytol. 196:177–244.
73. Yoshimura, T., Y. Kawano, N. Arimura, S. Kawabata, A. Kikuchi, and K. Kaibuchi. 2005. GSK-3beta regulates phosphorylation of CRMP-2 and neuronal polarity. Cell 120:137–149.
74. Yuan, X. B., M. Jin, X. Xu, Y. Q. Song, C. P. Wu, M. M. Poo, and S. Duan. 2003. Signalling and crosstalk of Rho GTPases in mediating axon guidance. Nat. Cell Biol. 5:38–45.
75. Yuasa-Kawada, J., R. Suzuki, F. Kano, T. Ohkawara, M. Murata, and M. Noda. 2003. Axonal morphogenesis controlled by antagonistic roles of two CRMP subtypes in microtubule organization. Eur. J. Neurosci. 17:2329–2343.
76. Zheng, J. Q., J. J. Wan, and M. M. Poo. 1996. Essential role of filopodia in chemotropic turning of nerve growth cone induced by a glutamate gradient. J. Neurosci. 16:1140–1149.

ent redundancy of these proteins has been suggested (Pollard, 2002). Organisms or cells that lack some actin crosslinking proteins still survive despite large defects in cell behavior and growth rate. *Dictyostelium* cells that lacked α-actinin showed no motility defects, with deficiencies only in behavior and architecture (Pollard, 2002; Rivero et al., 1996; Stossel et al., 2001). A cell line established from human malignant melanoma, which expressed no filamin, could not undergo locomotion in response to growth factors but was still able to survive (Stossel et al., 2001). These findings suggest that these crosslinking proteins share overlapping functions in the actin system, and that the inventory of important actin crosslinking proteins may still be incomplete (Pollard, 2002).

In this study, we identified a novel, to our knowledge, substrate of Akt. We designate it Girdin (girders of actin filaments), because RNA interference (RNAi)-mediated depletion of Girdin gives rise to the disruption of stress fibers and limited extension of lamellipodia in fibroblasts. A recently published paper also identified the same protein designated APE (Akt-phosphorylation enhancer) as an Akt binding protein (Anai et al., 2005), although a role in actin organization was not characterized. We show that the phosphorylation of Girdin/APE by Akt occurs at the leading edge of migrating cells, which controls the association between Girdin and the plasma membrane and subsequently facilitates the formation of lamellipodium.

Results

Identification of an Akt-Interacting Protein, Girdin/APE

To identify novel Akt substrates, we performed a yeast two-hybrid screen with full-length human Akt1 as bait and searched for interacting proteins by using a human fetal brain cDNA library. Two independent and overlapping clones (F-10 and F-12) encoding a novel gene product were identified. When expressed in yeast, the protein encoded by the F-10 and F-12 cDNAs was shown to interact only with the carboxyl-terminal regulatory domain (RD) of Akt1 (Figures 1A and 1B). Use of 5′-rapid amplification of cDNA ends (5′-RACE) provided a clone comprising the entire coding region with an additional 3.8 kb cDNA of contiguous 5′ sequence. The full-length cDNA included an open reading frame of 5610 base pairs (bp) and was predicted to encode a novel, to our knowledge, protein of 1870 amino acids, which we designated Girdin, with a calculated molecular mass of 220 kilodaltons (kDa) (Figure S1; see the Supplemental Data available with this article online). Database searches revealed homologs in mouse, rat, and *Drosophila* (not shown), but no apparent matches in *Caenorhabditis elegans* and *Dictyostelium*. A mouse ortholog of Girdin named APE was recently reported (Anai et al., 2005).

The structure of Girdin predicted by the COILS algorithm (Lupas et al., 1991) showed a tendency to assume an α-helical coiled-coil conformation in its middle domain, between Ala-253 and Lys-1375, with a high coiled-coil probability of 1.0 (Figure 1C). The predicted coiled-coil domain contains 135 continuous heptad repeats ($[abcdefg]_{135}$) that are typical of α-helical coiled-coils (Figure S1). The 9.5 kb Girdin transcript was found to be expressed ubiquitously in various human tissues by high-stringency Northern blot analysis (Figure 1D). To facilitate further studies on Girdin, we generated a polyclonal antibody (Ab) raised against its 19 C-terminal amino acids. Western blot analysis revealed that the anti-Girdin Ab recognizes a specific band of relative molecular mass of 250 kDa in human brain and testis lysates (Figure 1E).

Because of the existence of an α-helical coiled-coil domain in the primary structure of Girdin, we investigated the possibility of Girdin being an oligomeric molecule. Cell lysates from COS7 cells were analyzed by Western blot analysis with anti-Girdin Ab, either directly or after crosslinking with 100 μM Bis(sulfosuccinimidyl) suberate (BS^3) (Figure 1F). In the presence of BS^3, Girdin was predominantly found in a complex of large molecular mass. To determine the molecular mass of Girdin-containing protein complexes in intact cells, we subjected the lysates from COS7 cells to gel filtration (Figure S2). The data confirmed that Girdin forms a large protein complex. We next tested whether the NT and CT domains contribute to the oligomerization of Girdin. When V5 epitope-tagged NT (NT-V5) and myc epitope-tagged NT (NT-myc) were expressed in COS7 cells, a complex of these two NT domains was observed (Figure 1G). This result implies that the NT domain facilitates the oligomerization of Girdin. In contrast, the CT domain did not form an oligomer in cells (data not shown). Analysis of the lysates from COS7 cells expressing the NT domain by gel filtration suggested that the NT domain forms a dimer (Figure S2).

Akt Phosphorylates Girdin In Vitro and In Vivo

We initially used in vitro and in vivo assays to ascertain if Girdin and Akt physically interact with each other. Neither in vitro binding nor immunoprecipitation assays with various fragments of Girdin and Akt demonstrated the formation of a stable complex of the two proteins (data not shown), suggesting that they may normally associate in a very transient manner, as observed for the interactions between protein kinases and their substrates (Brazil et al., 2002). Although Anai et al. (2005) observed a weak association of the two proteins by immunoprecipitation, the difference may be due to the experimental conditions used.

It has been established that Akt preferentially phosphorylates substrates that contain the sequence R-x-R-x-x-S/T (Alessi et al., 1996). The amino acid sequence adjacent to a serine at position 1416 (Ser-1416 indicated by the underlined "S," RERQKS) in the CT domain of Girdin conforms to this consensus sequence (Figure 2Aa). This is the only consensus site in the protein. Since the CT domain with the putative phosphorylation site is conserved in different mammalian Girdin homologs (data not shown), we asked whether Akt phosphorylates Girdin. An in vitro kinase assay revealed that Girdin CT wild-type (WT), but not its Ser → Ala mutant (SA), was phosphorylated by active Akt, indicating that Akt directly phosphorylates the Ser-1416 in vitro (Figure 2Ab). In contrast, neither the NT nor the coiled-coil domain of Girdin was phosphorylated by Akt in vitro (Figure 2B).

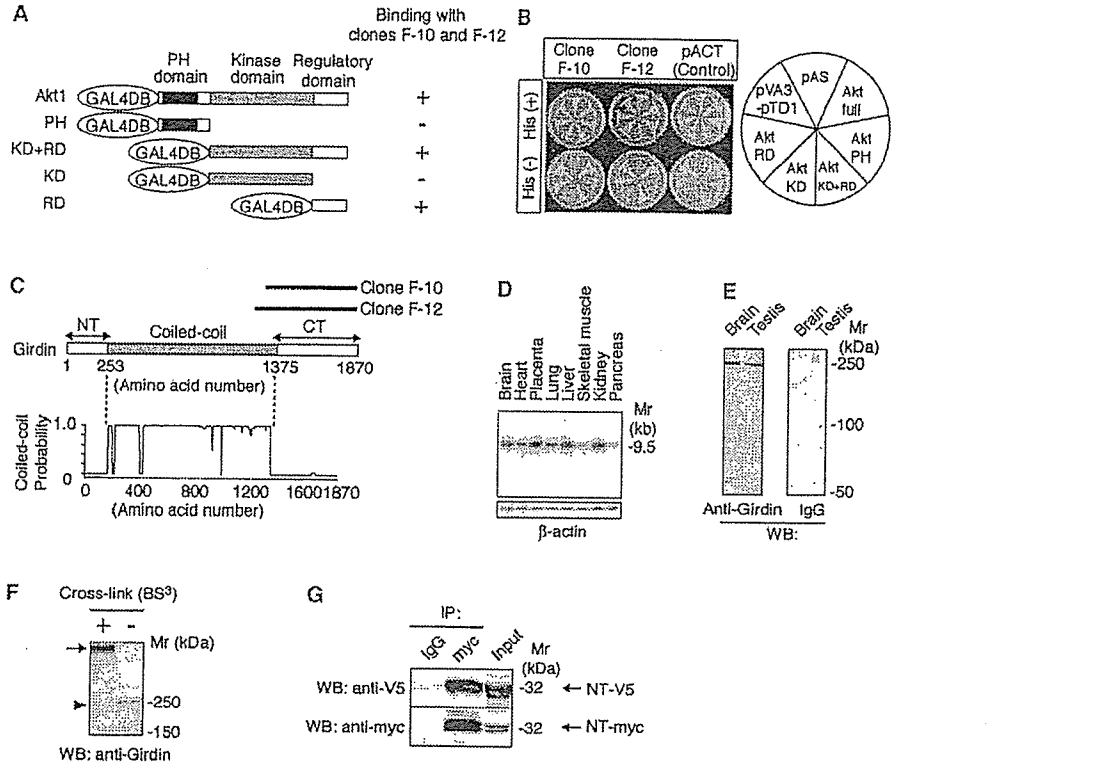

Figure 1. Identification, Primary Structure, and Expression of Girdin

(A) Schematic illustration of bait constructs for yeast two-hybrid binding assays. The cDNA fragments corresponding to the indicated domains of human Akt1 were fused in frame to the DNA binding domain of GAL4 transcription factor (GAL4DB) in the pAS2 vector. PH, pleckstrin homology domain; KD, catalytic kinase domain; RD, regulatory domain.

(B) Interactions of clones F-10 and F-12 with human Akt1 in yeast two-hybrid binding assays. pAS, a negative control; pVA3-pTD1, a positive control; His, histidine.

(C) Schematic presentation of Girdin and structure predictions provided by the COILS algorithm.

(D) Ubiquitous expression of Girdin mRNA in human adult tissues. A human multiple-tissue Northern (MTN) blot (Clontech) was hybridized with a probe corresponding to the 3′ region of Girdin cDNA.

(E) Endogenous Girdin in lysates from human brain and testis was detected with anti-Girdin polyclonal antibody, but not with rabbit IgG, under reducing conditions.

(F) Detection of a large complex formation by endogenous Girdin. COS7 postnuclear supernatants were subjected to Western blot analysis by using anti-Girdin antibody, either directly (–) or after crosslinking with 100 μM BS^3 (+). The size of a band detected after crosslinking (arrow) is extremely large compared with that without crosslinking (arrowhead).

(G) The NT domain of Girdin forms an oligomer. NT-V5 and NT-myc were transfected into COS7 cells and immunoprecipitated with anti-myc antibody. NT-V5 was coimmunoprecipitated with NT-myc. The multiple bands in the lower panel may represent the degradation of NT-myc in cells.

In order to confirm that Ser-1416 is the site of Akt-catalyzed phosphorylation in vivo, we raised an antibody to a peptide that includes phosphorylated Ser-1416 and used it for Western blotting (Figure 2C). The anti-phospho Ser-1416 peptide antibody (anti-P-Girdin Ab) recognized the Girdin CT (WT) that was coexpressed with wild-type (Akt WT) or constitutively active Akt (Akt CA), but not with dominant-negative Akt (Akt DN). The anti-P-Girdin Ab did not recognize the Girdin CT (SA) mutant coexpressed with the Akt CA. These findings indicate that the anti-P-Girdin Ab specifically recognizes the Girdin CT phosphorylated at Ser-1416.

We next asked whether the anti-P-Girdin Ab can detect the endogenous Girdin phosphorylated in response to external stimuli that physiologically activate endogenous Akt. As shown in Figure 2D, the addition of epidermal growth factor (EGF) induced the phosphorylation of a protein that corresponds to immunoprecipitated Girdin (250 kDa) with a time course similar to that of Akt activation. In addition, the phosphorylation of Girdin was inhibited when cells were treated with the PI3K inhibitors LY294002 and Wortmannin, but not with the mitogen-activated protein kinase kinase 1 (MEK1) inhibitor PD98059. We therefore concluded that the phosphorylation of Girdin is induced by EGF in a PI3K-dependent manner. The expression of Akt WT and Akt CA, but not Akt DN, induced significant phosphorylation of Girdin (Figure 2E), indicating that active Akt alone is sufficient to induce its phosphorylation in cells. Moreover, Girdin phosphorylation was undetectable in

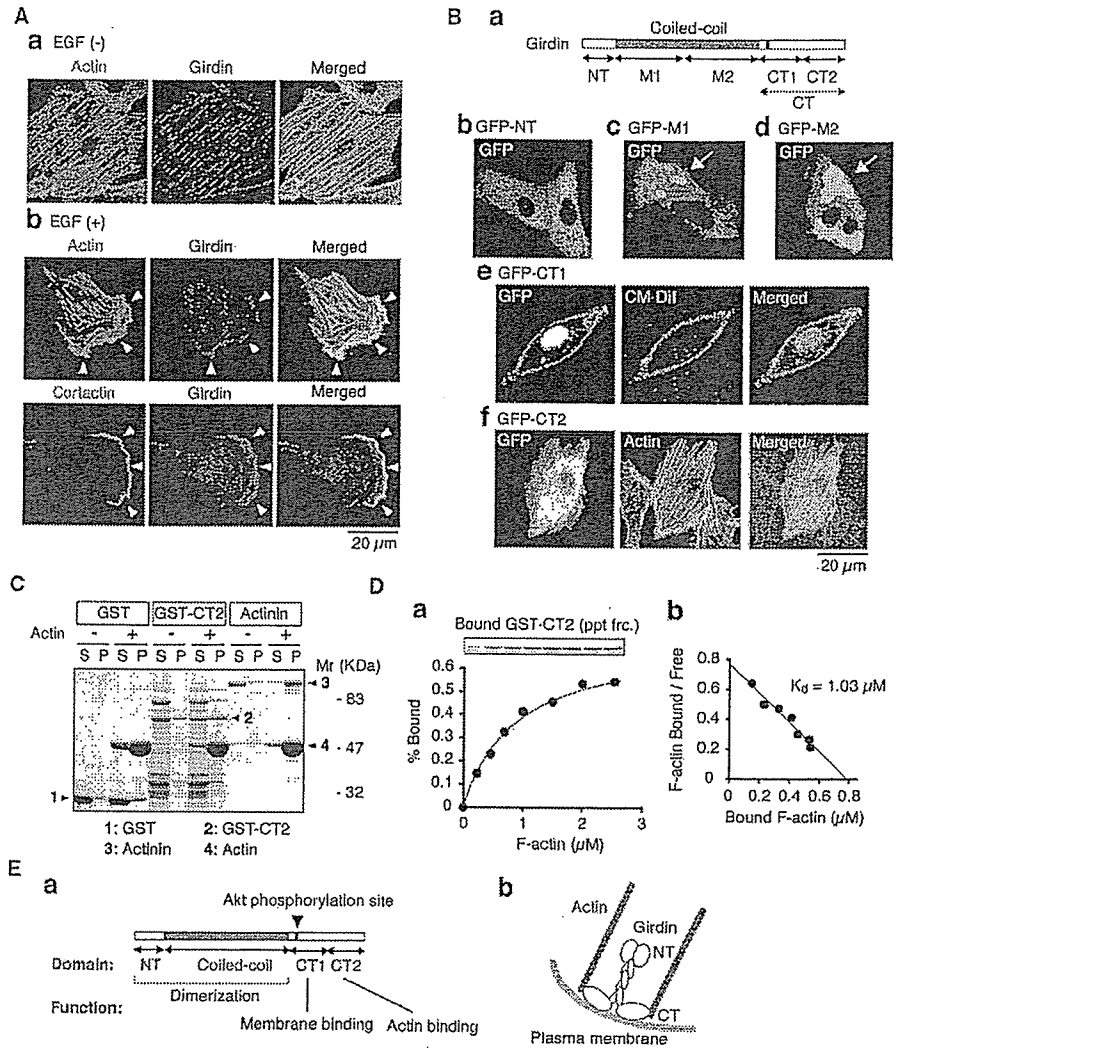

Figure 3. Girdin Binds to Actin Filaments through Its C-Terminal Domain

(A) (Aa) Quiescent or (Ab) EGF (50 ng/ml)-stimulated Vero cells were doubly stained with either Alexa488-phalloidin (upper panel) or anti-Cortactin antibody (lower panel) and anti-Girdin antibody. Arrowheads denote lamellipodia at the leading edge.

(B) Subcellular localization of Girdin fragments. Various fragments of Girdin (Ba) fused with GFP were expressed in Vero cells, fixed, and stained with the (Bb–Bf) indicated probes. Arrows denote aggregates of the expressed proteins. CM-DiI, Chloromethylbenzamido.

(C) Girdin CT2 directly interacts with filamentous actin in vitro. Purified GST (1), GST-CT2 (2), and α-actinin (3) were incubated with (+) or without (–) in vitro-prepared actin filaments (4). F-actin was subsequently pelletted by ultracentrifugation. Cosedimentation of the various proteins with F-actin was analyzed by CBB staining of the gel.

(D) Direct plot of binding of GST-CT2 to F-actin. A fixed amount of GST-CT2 (1 μM) was mixed with various amounts of F-actin (0–2.5 μM), followed by ultracentrifugation. Amounts of the free and bound GST-CT2 were quantified, and the (Da) percentage of bound GST-CT2 was plotted against the concentration of F-actin, and the (Db) K_d value was calculated by Scatchard analysis.

(E) (Ea) Summary of the localization and functions of Girdin domains. (Eb) The proposed structure of Girdin.

CT1) and the C-terminal half (GFP-CT2) of the CT domain, and we examined their intracellular localization (Figure 3Ba). When expressed in Vero cells, the GFP-NT, GFP-M1, and GFP-M2 localized in the cytoplasm (Figures 3Bb–3Bd). The GFP-CT1 localized in both the nucleus and the plasma membrane, as shown by its colocalization with CM-DiI, a carbocyanine membrane probe (Figure 3Be), while GFP-CT2 apparently localized on the stress fibers (Figure 3Bf). These findings suggest that Girdin localizes on the actin filament via its CT2 domain, whereas it also associates with the plasma membrane via its CT1 domain. The nuclear localization of the GFP-CT1 seen here may be an artifact, because no accumulation of endogenous Girdin was visible in the nucleus (Figure 3A).

We next investigated the actin binding properties of the CT2 domain by actin cosedimentation assays (Figures 3C and 3D). The purified glutathione S-transferase (GST)-fused CT2 (GST-CT2) cosedimented with purified F-actin, as did α-actinin, whereas GST alone did not

(Figure 3C), indicating that GST-CT2 directly binds to F-actin. As the amount of F-actin increased, the binding of GST-CT2 with F-actin was saturated (Figure 3Da). The estimated dissociation constant (K_d) for F-actin was 1.03 μM, indicating that Girdin has relatively low affinity for F-actin (Figure 3Db).

The domains of Girdin, their predicted functions, and the speculated structure of Girdin are summarized and illustrated in Figure 3E. Together, these findings allow us to propose that Girdin may possess an actin cross-linking property.

Girdin Is Required for the Formation of Actin Stress Fibers and Cell Migration

To assess the function of Girdin, we employed RNA-mediated interference (RNAi) to suppress (knockdown) the expression of Girdin in Vero cells. We introduced several Girdin small (21 nucleotide) interfering RNAs (Girdin siRNA) and a 21 nucleotide irrelevant RNAs (control siRNA) into Vero cells. Western blot analyses showed that transfection with the Girdin siRNAs effectively reduced the expression levels of Girdin by over 90% without affecting those of Akt and actin (Figure 4A). In order to verify the specificity of the knockdown experiments, the two oligonucleotides, Girdin siRNAs A and B, were utilized for Western blot analyses and other functional assays described in this study.

To test whether Girdin functions to promote the crosslinking of actin filaments, we examined the effects of Girdin knockdown on the organization of the actin cytoskeleton. Immunofluorescent staining with anti-Girdin Ab showed that the expression of Girdin was very low in the Girdin siRNA-transfected cells (Figure 4Bb). Staining of F-actin-rich structures with phalloidin revealed that the stress fibers were disrupted in the Girdin siRNA-transfected cells (Figure 4Bb), indicating that Girdin is essential for the formation of the stress fibers. When observed under higher magnification, Girdin siRNA-transfected cells contained markedly reduced thin and short stress fibers. Moreover, they lost their shape and formed with rugged boundaries that gave rise to the formation of multiple protrusions (leading edge) (Figure 4Bb, lower panel, and Figure 4C).

To further clarify the roles of Girdin in actin dynamics, we observed the behavior of the Girdin-depleted cells during migration in in vitro wound-healing assays (Figure 4D and Movies S1 and S2). We found that the Girdin siRNA-transfected cells facing the wound failed to produce extended lamellipodia at the leading edge and showed a migration defect that included multiple protrusions that were repeatedly stretched and shortened (Figure 4Db and Movie S2). These results suggest that Girdin is essential for organization of actin filaments during cell migration.

To test the specificity of the effect of the Girdin knockdown, we also introduced the Girdin siRNA into another cell line, SK-N-MC neuroblastoma cells, which stably express the RET receptor tyrosine kinase (Takahashi, 2001). Girdin siRNA-transfected SK-N-MC (RET) cells exhibited disruption of the stress fibers and limited formation of lamellipodia in response to the RET ligand, glial cell line-derived neurotrophic factor (GDNF) (Figure S3).

Localization of Girdin on Actin Filaments and Ultrastructure of the Girdin-Depleted Cells by Electron Microscopy

To further confirm the direct interaction of Girdin with actin filaments in vivo and its roles in actin organization, ultrastructural analysis was performed by deep-etch electron microscopy of "unroofed" Vero cells (Figure 5). Immunogold labeling revealed that Girdin molecules localize with actin filaments (Figure 5A). Higher-magnification views showed extensive colocalization of Girdin with the junctions between the actin filaments (Figure 5B).

Consistent with the immunofluorescence analysis, the density of the cortical actin filaments visible in electron micrographs of the cytoplasmic surface under the plasma membrane of Girdin-depleted Vero cells is lower than that in the control cells, where more tightly organized actin fibers predominate (Figure 5C). In the control siRNA-transfected cells, the filaments abut one another, run together without separating, and form thick cables tightly crosslinked by many molecules. Some filaments were oriented perpendicular to the other actin cables, resulting in interwoven and dense actin networks. In the Girdin siRNA-transfected cells, however, the actin bundles are sparse, and each actin filament is separated from another and is sometimes disrupted en route.

Phosphorylated Girdin Localizes to the Leading Edge of Migrating Cells

To gain insight into the role of Girdin phosphorylation by Akt, we examined the location of phosphorylated Girdin in Vero cells by staining with the anti-P-Girdin Ab (Figure 6A). In serum-starved quiescent cells, phosphorylation of Girdin was hardly detected throughout the cells (Figure 6A, top panel), consistent with the results of Western blot analyses (Figure 2D). When cells were stimulated with EGF (50 ng/ml), the immunostaining showed that phosphorylated Girdin appeared in the lamellipodia at the leading edge of migrating cells (Figure 6A, middle panel). The phosphorylated Girdin was also colocalized with Cortactin that exists at the leading edge (Figure 6B). Moreover, we observed that the stimulation of Vero cells with EGF enhanced the specific accumulation and localization of active Akt with phosphorylated Girdin in lamellipodia at the leading edge (Figure S4). In the Girdin siRNA-transfected cells, stimulation by EGF induced multiple leading edges. At these leading edges, the signals of phosphorylated Girdin were abolished as expected (Figure 6A, bottom panel), further supporting the specificity of the immunostaining. The nuclear signal seen in the immunostaining was still visible in the Girdin siRNA-transfected cells (Figure 6A, bottom panel), indicating that it was an artifact.

Akt Regulates the Association of Girdin with the Plasma Membrane

What is the mechanism that determines localization differences between the phosphorylated and nonphosphorylated forms of Girdin? Because the CT1 domain of Girdin localizes to the plasma membrane and contains the phosphorylation site, we hypothesized that it is the association of Girdin with the plasma membrane

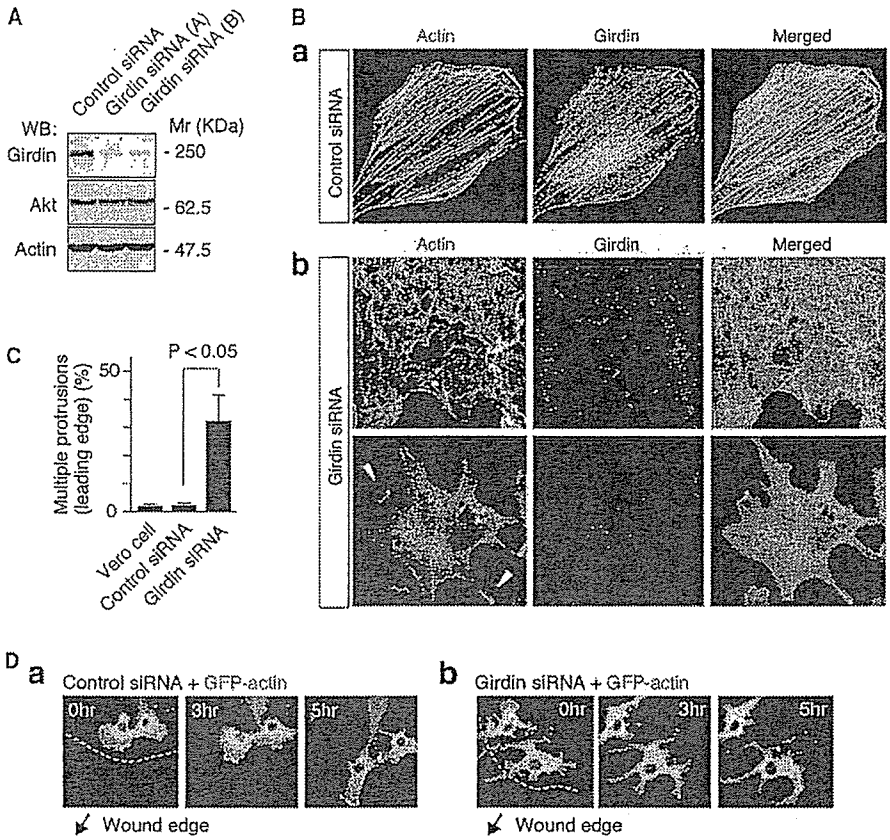

Figure 4. Girdin Is Essential for the Formation of Stress Fibers and Cell Migration

(A) Depletion of Girdin in Vero cells by siRNA. Total cell extracts from control siRNA- and Girdin siRNA-transfected Vero cells were subjected to Western blot analyses with anti-Girdin, anti-Akt, and anti-actin antibodies.

(B) Vero cells were transfected with (Ba) control or (Bb) Girdin siRNAs and fixed 72 hr after transfection, followed by staining with Alexa488-phalloidin and anti-Girdin antibody. Arrowheads denote lamellipodia at the tips of protrusions.

(C) After transfection of each siRNA, the number of cells with multiple protrusions was counted by staining with anti-Girdin antibody and Alexa488-phalloidin. More than 100 transfected cells were counted in each group. The results represent the means ± SE.

(D) Vero cells were cotransfected with GFP-actin and either (Da) control or (Db) Girdin siRNA and incubated for 48 hr. Cells were plated on fibronectin-coated glass coverslips and wounded to induce cell migration. Images were collected every 90 s for a period of 5–6 hr starting 2 hr after scraping. The arrows indicate the direction of cell migration into the wounds.

that is regulated by the phosphorylation. We found that a positively charged sequence of 19 amino acid residues (Arg-1389 to Lys-1407) upstream of the phosphorylation site (Figure 6Ca) resembles a consensus sequence for phosphatidylinositol 4,5-bisphosphate (PI[4,5]P2) binding (Sechi and Wehland, 2000). When the GFP-CT1 in which the phosphoinositide binding site was deleted (termed GFP-CT1 ΔPB) was transfected into Vero cells, localization of GFP-CT1 ΔPB to the plasma membrane was not observed (Figure 6Cb). This finding suggested that the CT1 domain is anchored at the plasma membrane through binding to phosphoinositides.

To examine the phosphoinositide binding properties of Girdin, we performed a protein-lipid binding assay with purified GST fusion proteins containing the phosphoinositide binding site of Girdin (Figures 6D and 6E). In the experiment, we utilized the CT domain fused with GST instead of the CT1 domain (Figure 6Da), because the GST-CT1 fusion protein was easily degraded during expression and purification procedures. As shown in Figure 6Ea, GST-CT bound selectively to PI(4)P and weakly to PI(3)P, but to none of the other phosphoinositides or phospholipids. The binding property of GST-CT to PI(4)P and PI(3)P was abrogated when the phosphoinositide binding site was deleted (Figure 6Eb). We also found that mutants of the CT1 domain, in which the positively charged basic residues were replaced with alanines (Girdin PBala mutant), failed to bind to the phosphoinositides and were delocalized from the plasma membrane (Figure S5), suggesting that the positive electrostatic charge generated by the basic residues in the phosphoinositide binding motif is required for the association of Girdin with the plasma membrane.

Since the phosphoinositide binding site is located near the Akt phosphorylation site (Figure 6Ca), the sup-

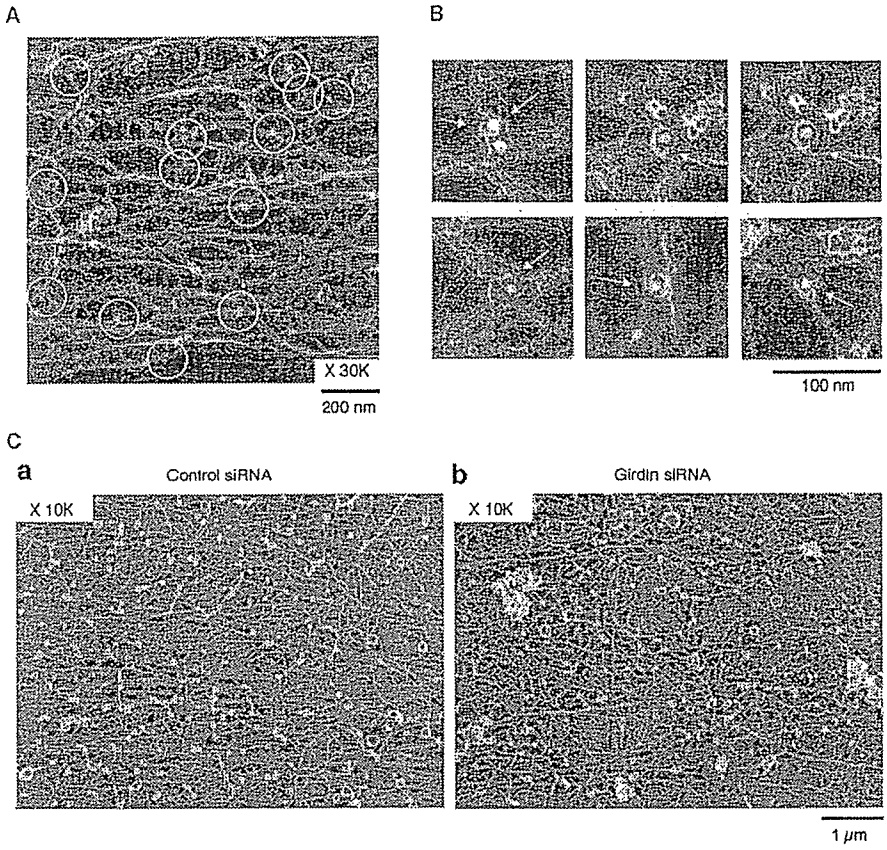

Figure 5. Electron Microscopic Analysis of Girdin Localization and the Effect of Its Depletion on Actin Organization

(A) Immunogold electron microscopy with anti-Girdin antibody.

(B) Circles indicate the immunogold signals of Girdin molecules, shown here under higher magnification. Arrows denote the immunogold signals.

(C) Ultrastructure of actin filaments in Vero cells transfected with either (Ca) control or (Cb) Girdin siRNA.

position was made that Akt might control the localization of Girdin by regulation of its phosphoinositide binding property. To determine if this is the case, we examined the phosphoinositide binding property of phosphorylated GST-CT. Purified GST-CT was effectively phosphorylated by Akt in vitro (Figure 6Db). GST-CT was then subjected to the protein-lipid binding assay, in which binding was detected by anti-P-Girdin Ab. As shown in Figure 6Ec, the phosphorylated GST-CT bound to neither PI(4)P nor PI(3)P. In addition, actin cosedimentation assays showed that the phosphorylation of GST-CT did not attenuate its affinity for F-actin (Figure 6F), and that the binding kinetics was similar to that of GST-CT2 (Figure 3D). These findings suggested that the binding of Girdin to the phosphoinositides, but not to F-actin, is attenuated by phosphorylation.

Moreover, we investigate whether the membrane association of Girdin is regulated by EGF treatment, by using COS7 cells expressing either the GFP-full-length Girdin WT or SA mutant. The results supported the view that phosphorylation at Ser-1416 by Akt is necessary for the delocalization of Girdin from the plasma membrane. (Figure S6).

Phosphorylation of Girdin by Akt Is Required for Cell Migration

The localization of phosphorylated Girdin at the leading edge prompted us to test whether the phosphorylation of Girdin is involved in cell motility. After wounding a confluent monolayer of Vero cells, immunostaining with anti-P-Girdin Ab showed that the level of Girdin phosphorylation in cells at the wound edge increased soon after scratching, reached a maximum at 8 hr, and lasted for at least 12 hr (Figure 7A). The implication is that the phosphorylation of Girdin may play an important role in cell motility. Thus, the role of Girdin in cell motility was examined with Boyden chamber assays. The Girdin knockdown significantly retarded the ability of Vero cells to migrate in response to EGF (50 ng/ml) added to the lower chamber (Figure 7B). We also found that expression of the CT domain in Vero cells significantly attenuated cell migration (Figure 7B), supporting the